Mon. Not. R. Astron. Soc. **000**, ??–?? (2014) Printed 27 October 2015 (MN LATEX style file v2.2)

Kinematics of dwarf galaxies in gas-rich groups, and the survival and detectability of tidal dwarf galaxies.

Sarah M. Sweet[1*], Michael J. Drinkwater[2], Gerhardt Meurer[3,4], Virginia Kilborn[5], Fiona Audcent-Ross[3,4], Holger Baumgardt[2], Kenji Bekki[3,4]

1: Research School of Astronomy and Astrophysics, The Australian National University, Cotter Road, Weston Creek, ACT 2611, Australia;
2: School of Mathematics and Physics, University of Queensland, Qld, 4072, Australia;
3: School of Physics, University of Western Australia, 35 Stirling Highway, Crawley, WA, 6009, Australia;
4: International Centre for Radio Astronomy Research, ICRAR M468, 35 Stirling Highway, Crawley, WA, 6009, Australia;
5: Centre for Astrophysics & Supercomputing, Swinburne University of Technology, Mail number H30, PO Box 218, Hawthorn, Victoria 3122, Australi
** sarah@sarahsweet.com.au*

arXiv:1510.07206v1 [astro-ph.GA] 25 Oct 2015

27 October 2015

ABSTRACT

We present DEIMOS multi-object spectroscopy (MOS) of 22 star-forming dwarf galaxies located in four gas-rich groups, including six newly-discovered dwarfs. Two of the galaxies are strong tidal dwarf galaxy (TDG) candidates based on our luminosity-metallicity relation definition. We model the rotation curves of these galaxies. Our sample shows low mass-to-light ratios (M/L=0.73±0.39$M_{\odot}/L_{\odot}$) as expected for young, star-forming dwarfs. One of the galaxies in our sample has an apparently strongly-falling rotation curve, reaching zero rotational velocity outside the turnover radius of $r_{turn} = 1.2r_e$. This may be 1) a polar ring galaxy, with a tilted bar within a face-on disk; 2) a kinematic warp. These scenarios are indistinguishable with our current data due to limitations of slit alignment inherent to MOS-mode observations. We consider whether TDGs can be detected based on their tidal radius, beyond which tidal stripping removes kinematic tracers such as Hα emission. When the tidal radius is less than about twice the turnover radius, the expected falling rotation curve cannot be reliably measured. This is problematic for as much as half of our sample, and indeed more generally, galaxies in groups like these. Further to this, the Hα light that remains must be sufficiently bright to be detected; this is only the case for three (14%) galaxies in our sample. We conclude that the falling rotation curves expected of tidal dwarf galaxies are intrinsically difficult to detect.

Key words: galaxies: groups – galaxies: dwarf – galaxies: mass – galaxies: mass-to-light ratios – galaxies: dark matter – galaxies: kinematics

1 INTRODUCTION

Occupying the low-mass end of the galaxy mass function, dwarf galaxies are more numerous than their giant counterparts (e.g. Bell et al. 2003; Oppenheimer et al. 2010), and as such can be an important tracer of environmental effects (e.g. Drinkwater et al. 2003). Moreover, the contribution by dwarf galaxies to hierarchical assembly and accretion onto giant galaxies is a vital part of our understanding of galaxy formation (e.g. Searle & Zinn 1978, and many observational and theoretical works since). In ΛCDM cosmology, galaxies form in haloes of cold dark matter (DM, Peebles 1965; Press & Schechter 1974; Blumenthal et al. 1984). These galaxies assemble into larger galaxies within still-larger haloes, which contribute a high M/L ratio and flat rotation curve for all galaxy masses (e.g. Navarro 1998; Klypin et al. 2002). At the same time, continual enrichment of the inter-stellar medium means that larger galaxies have higher metallicities (e.g. Lequeux et al. 1979; Tremonti et al. 2004).

Galaxy groups are ideal laboratories for the study of dwarf galaxies, as it is at this density that the environment begins to contribute to their evolution. Moreover, the harsh conditions caused by galaxy clusters are not present, so that galaxy harassment is less frequent (Lewis et al. 2002; Gómez et al. 2003). Interactions between giant galaxies in such groups can cause the necessary Jeans instabilities for small galaxies to form in the tidal debris (Bournaud 2010). These so-called tidal dwarf galaxies (TDGs) share the high metallicity of the giant galaxies from which they formed, so are unusually metal-rich for their small size (e.g. Mirabel et al. 1992; Duc et al. 2000; Weilbacher et al. 2003). They also have no or little non-baryonic DM, though may contain a significant fraction of baryonic DM (Bournaud et al. 2007).

© 2014 RAS

Notwithstanding, they have a low M/L ratio (e.g. Braine et al. 2001) and are expected to have a falling, mass-follows-light rotation curve (e.g. Bournaud 2010; Duc et al. 2014). Understanding the fraction of dwarf galaxies that form in a tidal manner instead of in the traditional hierarchical assembly paradigm is crucial to instructing cosmological simulations.

Most TDGs discovered to date have been detected due to their location in the tidal streams in which they form (e.g. Mirabel et al. 1992; Duc et al. 2000; Weilbacher et al. 2003; Duc et al. 2011, 2014). However, the same streams that identify these objects as TDGs also indicate tidal distortion of their velocity fields, so that dynamical masses cannot be reliably measured, nor can the presence or absence of DM be determined (Casas et al. 2012). For example, dwarf galaxies in obviously interacting systems such as the Perseus Cluster have comparable M/L ratios ($\sim$120 $M_\odot/L_\odot$) to the CDM dwarf satellites of the Milky Way (Penny et al. 2009). The exception to this problem is where tidal streams are old and faded, as in Duc et al. (2014), and the TDG has had time to reach dynamical equilibrium.

The aim of this paper is firstly to detect TDGs based on their elevated metallicity and falling rotation curve alone, without the presence of tidal streams that confuse kinematic measurements. To that end, here we present rotation curves and metallicities for a sample of star-forming dwarfs in gas-rich galaxy groups, many of which do not have obvious evidence of tidal streams. Section 2 outlines our sample selection, observations and data processing. In Section 3 we present our results, including rotation curve modelling, mass-to-light ratio, and one rapidly-falling rotation curve. Finding that the rotation curves of many galaxies in the sample are distorted even without the presence of obvious tidal streams, in Section 4 we discuss the survival and detectability of TDGs in the group environment; this is the second main aim of the paper. Section 5 concludes the paper. The Appendices contain notes on and rotation curves for individual galaxies in the sample.

2 SAMPLE SELECTION, OBSERVATIONS AND DATA PROCESSING

Our sample consists of dwarf galaxies within the star-forming, gas-rich groups known as Choirs (Sweet et al. 2013). These fifteen groups of four or more Hα emission line galaxies were detected in the Survey for Ionisation in Neutral Gas Galaxies (SINGG Meurer et al. 2006), a follow-up Hα imaging survey to the HI Parkes All Sky Survey (HIPASS Barnes et al. 2001).

In Sweet et al. (2014) we presented ANU 2.3-m WiFeS (Dopita et al. 2007) integral field spectroscopy for 53 galaxies in eight of these Choir groups. We measured spatially-integrated metallicities for that sample in order to identify a sample of tidal dwarf galaxy (TDG) candidates based on elevated metallicity for their *R*-band magnitude. To confirm whether or not they are true TDGs we set out to measure their rotation curves; a falling rotation curve would demonstrate the absence of a dark matter halo as expected for such galaxies. However, with the small telescope aperture we do not enjoy sufficient signal-to-noise to allow resolved kinematic analyses of the faint dwarfs in the sample.

We therefore obtained Keck DEIMOS (Faber et al. 2003) spectroscopy for four Choir groups on 2013 February 11 ; two groups (J1051-17 and J1403-06) from our WiFeS sample and two new groups (J0443-05 and J1059-09), being sources with observable right ascensions during the allocated observing date. We used the 1200L grating with central wavelength 5950 Å and the GG400 order-blocking filter. Each group was observed for six 1200-s exposures. Mask and slit placements are shown in Appendix C. We chose the mask position angle to facilitate observing as many of our Choir member galaxies as possible. The remaining spare mask area was used to allocate slits to other sources suggestive of some net Hα emission in the SINGG imaging but not already identified, with the intention of detecting new group member galaxies. This selection expanded our sample to $\sim$100 objects per mask.

Data processing was conducted using the DEIMOS DEEP2 data reduction pipeline[1]. This pipeline is optimised for compact sources observed with a central wavelength of around 7700 Å, so we employed Evan Kirby's modification[2] to enable processing of our bluer wavelengths. We also modified the sky subtraction routines to give more flexibility for extended sources, as most of our galaxies are sufficiently extended to fill their slits. In these cases we selected a section of another slit that contains some sky to perform a non-local sky subtraction. While there is some residual sky emission due to variations in the observed sky spectrum caused by slit angle and width differences and path through the optics and detector, the residual sky emission does not overlap with the Hα for the redshifts of our groups, so the result is adequate for velocity measurements.

We used our own software to extract a portion of the spectrum at the expected Hα wavelength for each row of binned pixels, and fit a single Gaussian profile to the peak to measure redshift. There is no evidence for multiple components at the resolution of our data. The peak location error from the χ^2-minimisation fit is used to derive the 1-σ observed velocity errors quoted herein. The Hα width and flux and continuum flux were also measured for each bin. In order to measure the true profile width, the spectrum cutout was deconvolved with a line spread function (LSF) measured from a nearby bright sky line. Importantly, we noticed that the LSF varied significantly with the tilt and location of the slit on the mask, so we chose a sky line in each slit for the LSF measurement. Heliocentric velocity corrections were calculated using the IRAF package RVCORRECT. Our measurements confirm that six of the potential member galaxies in two groups lie at the group redshift; these are included in Table 1. We used the methods outlined in Meurer et al. (2006) to measure these new galaxies' extinction-corrected R-band magnitudes, surface brightness profiles and effective radii from the SINGG imaging.

We observed one spectrophotometric standard star for each

[1] http://www2.keck.hawaii.edu/inst/deimos/pipeline.html
[2] http://www2.keck.hawaii.edu/inst/deimos/calib_blue.html

mask and performed flux calibration in the standard manner.

We measured the integrated metallicity of each galaxy by collapsing spectra in the spatial direction and fitting a Gaussian profile to these integrated spectra to measure strong emission line fluxes. The wavelength range of DEIMOS 1200L grating with our central wavelength covers most of the necessary strong emission lines for using the Dopita et al. (2013) [NII]/[SII] vs. [OIII]/[SII] diagnostic. This is the same calibration as used in Sweet et al. (2014); we give a discussion of our reasons for choosing it in that paper. Briefly, this diagnostic gives consistent results with recombination and electron temperature methods; the necessary lines are available in most of our sample; and is not degenerate, clearly separating ionization parameter and metallicity: the [NII]/[SII] ratio is sensitive to metallicity, while the [OIII]/[SII] ratio tells the dependence on ionization parameter. The metallicities derived from the DEIMOS data are not corrected for reddening in most cases, because most do not have measurable Hβ, with the line either lost in the noise of the blue end, or fallen off of the chip. In any case, the diagnostic is not very dependent on reddening: because the [NII] and [SII] lines are nearby in wavelength, the [NII]/[SII] ratio will not vary much with reddening.

For the galaxies with all three strong emission lines available, we use the methods described in Sweet et al. (2014) to interpolate for metallicity and ionization parameter log(q). For the galaxies with only [NII] and [SII] available, we roughly estimated the ionization parameter log(q) based on a polynomial fit to log(q) as a function of R-band absolute magnitude M_R of the DEIMOS galaxies for which all three strong lines are available; $\log(q) = 10.836 + 0.3593M_R + 8.361x10^{-3}xM_R^2$. We then used [NII]/[SII] and log(q) to estimate 12 + log(O/H) by inspection of the same diagnostic. These measurements are therefore less reliable and have a nominal 0.5 dex error bar to show this. While the [NII]/[SII] ratio alone has a similar scatter to the [NII]/Hα calibration (e.g. Marino et al. 2013), the method just described has the added benefit of providing log(q), which gives a better constraint on the metallicity. The metallicity measurements are catalogued in Table 1.

3 RESULTS AND ANALYSIS

Our first step towards identifying TDGs aside from their location in a tidal stream is to select candidates based on their elevated metallicity; the second is to confirm the absence of dark matter by measuring a falling rotation curve. In this section we employ that method, firstly presenting our sample of dwarf galaxies on the luminosity-metallicity relation, and then modelling their rotation curves. We then measure mass-to-light ratios for those galaxies where this can be reliably obtained. The section finishes with a discussion of one galaxy with an apparently strongly-falling rotation curve.

3.1 Luminosity-metallicity relation

In Figure 1 we plot the luminosity-metallicity relation for our full sample of WiFeS (Sweet et al. 2014) and DEIMOS (this work) measurements. In general, the galaxies with DEIMOS measurements are consistent with the portion of our sample for which we have WiFeS measurements, and with the SDSS relation defined in Sweet et al. (2014). In that paper we identified a metallicity floor for low luminosity galaxies in SDSS. There is a suggestion of the metallicity floor being continued to fainter magnitudes by the new measurements.

We select TDG candidates in the DEIMOS data based on our definition from Sweet et al. (2014) (12+log(O/H)>8.6 and more than 3σ above SDSS); these are J1051-17:g11 and J1403-06:g1. However, J1403-06:g1 lies in the halo of its host spiral, and is probably experiencing strong tidal interactions, so is not detectable as a TDG based on its velocity profile (see Section 4).

Six of the galaxies in our sample have both WiFeS and DEIMOS metallicity measurements. In the J1403-06 group these metallicities agree to within quoted errors, even without [OIII] for the DEIMOS measurements. However, the J1051-17 group members where we can compare the data generally do not have consistent metallicities between DEIMOS and WiFeS, separated by up to 2σ. This is partly due to the missing [OIII] line for some of the DEIMOS measurements, but more generally because bright sky lines fall on the [SII] lines at the distance of this group. There is some unavoidable sky residual for both instruments due to the non-local sky subtraction employed. The sky residuals therefore contribute to the [SII] flux measurements and skew the metallicities for this group. We expect that the DEIMOS sky subtraction discussed above may be worse than for the WiFeS observations, where we used a nod-and-shuffle technique which minimised systematics related to optics and detector position.

3.2 Rotation curve modelling

We constructed rotation curves along the DEIMOS slit for each of the galaxies in our sample. We defined the zero velocity point as the velocity at the bin with the maximum continuum flux. This centre is a reasonable match to optical SINGG isophotal measurement of the centre for most of the galaxies in the sample. For J0443-05:S3 there are bad rows very near the centre of the galaxy, so for this galaxy we fit the centre by eye, assuming a symmetrical mass distribution. The rotation curve for one of the the more interesting galaxies in our sample, J0443-05:S4, is shown in Figure 2 and discussed further in Section 3.5. Rotation curves for the other galaxies in our sample, along with notes on each, are presented in Appendices A and B.

We test for the absence of DM by modelling the rotation curves of these galaxies. If the observed rotation curve is consistent with a mass-follows-light profile instead of being flat, then DM is not required to explain the rotational velocity. We assume an exponential disk and use the analytical

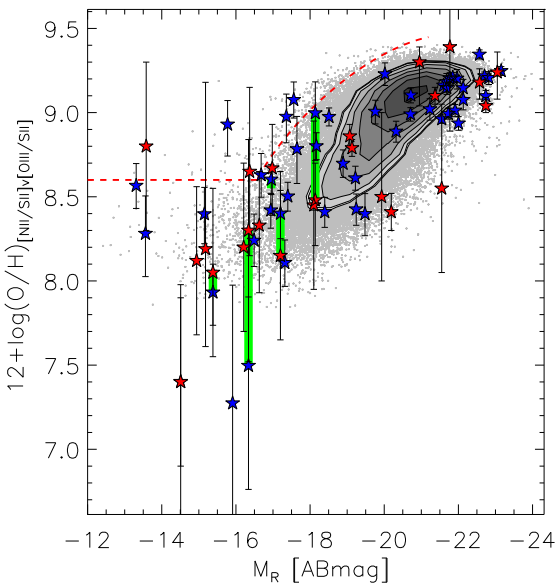

Figure 1. Luminosity-metallicity relation for the full sample of galaxies. Blue stars are existing WiFeS measurements from Sweet et al. (2014). Red stars are DEIMOS measurements. Green bars connect WiFeS and DEIMOS metallicities for five of the six galaxies that have measurements from both instruments; both measurements for J1403-06:S4 at $M_R = -14.51$ are equal. Grey points and contours depict SDSS star-forming galaxies, while the red, dashed line indicates our strong TDG candidate diagnostic. Galaxies above this line are more than 3 sigma above the typical metallicity for their luminosity and hence candidate TDGs.

prescriptions of Freeman (1970) for this modelling: the predicted rotational velocity for a mass-follows-light system is given by $v_{rot}^2 = \pi G \mu_0 r^2 (I_0 K_0 - I_1 K_1)$. Here, $\mu_0 = M/L \times S_0$ is the central surface density, M/L is the mass-to-light ratio and S_0 is the central surface luminosity. $I_{0(1)}$ and $K_{0(1)}$ are modified Bessel functions of the zeroth (first) kind evaluated at $\frac{r}{2r_0}$, where r_0 is the scale length. This mass-follows-light profile is akin to a Keplerian falloff beyond the turnover radius $r_{turn} = 2r_0 = 1.2r_e$, where r_e is the R-band effective radius. (This is for a purely exponential galaxy; for a bulge-dominated galaxy the turnover will be at a smaller multiple of r_e.) Our measurements of μ_0 and r_0 are derived assuming pure exponential disks from the effective surface brightness and radius measurements in the R-band, as described in Meurer et al. (2006).

We corrected for inclination using the optical axial ratio b/a from SINGG photometry, where b is the semi-minor axis and a is the semi-major axis, and the angle of inclination i is given by $\cos(\mathrm{i} - 3^\circ) = \sqrt{((\mathrm{b/a})^2 - 0.2^2)/(1 - 0.2^2)}$, the factor of 0.2 is a correction for disk thickness (Tully & Fisher 1977) and 3° is an empirical correction for the difference in the flattening of stellar vs. HI disks (Aaronson et al. 1980). We also corrected for angle of misalignment ϕ between slit position angle and SINGG optical major axis position angle. The misalignment is a function of the chosen slit mask position angle and the constraints of the instrument; the slit position angle (PA) must be $5^\circ < |PA| < 30^\circ$ with respect to the mask, limiting the choice of position angle. The model rotation curve obtained from fitting the optical data is divided by the total correction of $\sin(i)\cos(\phi)$.

We do not have sufficient information to model the asymmetric drift. While we have measured the Hα velocity dispersion at each point in our spectra, this emission is strongly affected by HII regions. It is not clear that these are in virial equilibrium, since their dynamics are thought to be dominated by short-lived ($\lesssim$ 10 Myr) expansion from ionisation, stellar winds and supernovae (Shopbell & Bland-Hawthorn 1998; Clarke & Oey 2002). The nature of the diffuse ionised gas Hα between HII regions is also unclear, and in many cases is a signature of outflows such as galactic winds (Oey et al. 2007; Rodríguez-González et al. 2008). We also do not have sufficient information about the neutral and molecular ISM (which is being ionised to become Hα) to determine its contribution: our HI data has insufficient resolution, and we have no molecular observations. We can estimate the order of magnitude of the asymmetric drift as follows (noting that this estimate is an upper limit, since the dispersion in the Hα emission is overestimated for the reasons just mentioned). The asymmetric drift correction term σ_D as a function of radius r is given by $\sigma_D^2 = -r\sigma^2[\partial ln(\Sigma_g)/\partial r + 2\partial ln(\sigma)/\partial r - \partial ln(h_z)/\partial r]$, where σ is the Gaussian sigma of the 1D Hα velocity profile measured as described in the previous section, h_z is the vertical scale height of the disk and Σ_g is the gas surface density. For most of the galaxies in the sample there is no obvious dependence of σ on the radius, so we adopt a single median value for each galaxy, with a sample mean of 20 km s^{-1}. We also assume that h_z is constant with radius, so the correction term becomes simply $\sigma_D^2 = -r\sigma^2[\partial ln(\Sigma_g)/\partial r]$. Making a further assumption that the ionised gas distribution is similar to the neutral gas and star distributions allows fitting an exponential profile to the natural log-scaled continuum flux as a function of r. Doing so results in a mean asymmetric drift correction of around 6 km s^{-1} at maximum velocity. As this is a simplified estimation only, we do not include this correction in our further analysis.

3.3 Rotation curve quality

Reliable mass-to-light ratios are dependent on good quality observations. Unfortunately, not many of the rotation curves in this sample are simple to analyse: several are disturbed, having asymmetric velocity profiles, and others have multiple SF regions or possible counter-rotating cores. In our case we restrict our M/L analysis to the galaxies that meet the following criteria:

(i) $\sin(i)\cos(\phi) > 0.4$, so there is neither a large correction for galaxy inclination nor misalignment between the slit and galaxy position angle; and,

(ii) sufficiently large and bright so that the photometry is reliable (this cutoff is effectively between galaxies in the original SINGG sample and fainter galaxies identified in this work); and,

(iii) not strongly disturbed in appearance (e.g. Fig. B11).

The resulting sample, which we label Sample A, consists of ten dwarf galaxies, out of 22 for which we have DEIMOS

measurements. The galaxies within Sample A are indicated in Table 1.

The fraction of our sample that meets criterion (i) is 60% (all of the galaxies in Sample A, plus three that fail criteria (ii) and (iii)). We can calculate the expected fraction that meets the first criterion as follows. The position angle misalignment is given by $\phi = PA - 30^\circ$, where the galaxy position angle with respect to the mask is $30^\circ \leqslant PA \leqslant 90^\circ$. and $\phi = 0^\circ$ for $0^\circ \leqslant PA < 30^\circ$. For a randomly-oriented galaxy, a PA of 45° then gives a median $\phi = 15^\circ$. Half of a sample of such galaxies should therefore have $\phi \leqslant 15^\circ$. Solving $\sin(i)\cos(15^\circ) > 0.4$ for i gives a minimum inclination of 23°, below which the amplitude in the rotation curve rapidly becomes too low to measure. For a randomly-selected sample, the frequency of any given cos(inclination) should be constant, so up to $\sim\cos(23^\circ) = 92\%$ of galaxies are more edge-on than this. The resulting expected fraction of galaxies that meets our first criterion is therefore 0.5 x 0.92 = 46%; considerably lower than the 60% in our sample. The position angle calculations rely on our assumption of disk-like systems. However, the irregular galaxies may be better modelled as triaxial systems, which are more prolate. This means that there is a lower chance of observing these to be circular and measuring low, face-on inclinations in the disk-like model (van den Bergh 1988), so much of the difference between the expected and observed fraction of edge-on galaxies is likely attributable to triaxiality of the irregular galaxies. In addition to this, we also expect that there are group effects causing a non-random orientation in position angles in our sample. In particular, there is a hint of a stream of dwarf galaxies in J1051-17 (see Fig. C2), which is to be discussed in a forthcoming paper (Kilborn et al., 2015, in prep.).

3.4 M/L ratios

We test for the presence of DM by calculating M/L ratios through fitting model curves to observed rotational velocities as described above. A high M/L ratio implies the presence of DM and a normal hierarchical formation mechanism. In general the M/L ratios in Sample A are low, but not dramatically so, at a mean M/L ratio of $0.73 M_\odot/L_\odot$ and standard error on the mean of $\pm 0.39 M_\odot/L_\odot$. Low M/L ratios in general simply confirm that these are young galaxies forming stars. Some of our wider sample does not have sufficient signal at radii $> r_{turn}$, so that our modelling calculates lower limits on masses and mass-to-light ratios. However, this does not significantly affect Sample A, which all have reliable measurements within r_{turn} and are well-modelled.

We plot M/L ratios as a function of the luminosity-metallicity relation using Sample A in Fig. 3. While sparse, the data suggest a trend towards higher mass-to-light ratios with higher luminosity. This is consistent with the view that the luminosity-metallicity relation arises from the deeper potential well of larger galaxies, which makes them more able to retain metal-rich supernovae ejecta (Gibson & Matteucci 1997; Kauffmann et al. 2003).

Unfortunately, neither of the strong TDG candidates identified above is part of Sample A, so we cannot include either

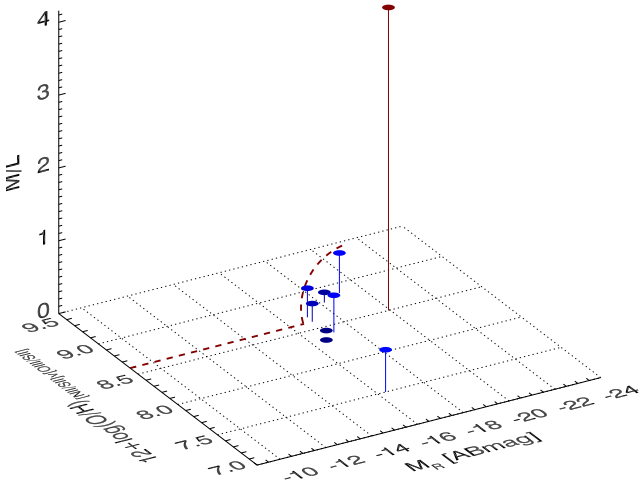

Figure 3. Mass-to-light ratio as a function of the luminosity-metallicity relation for the galaxies in our sample that have reliable mass-to-light ratios. The data points are colour-coded by mass-to-light ratio, with red being the highest and blue the lowest in this sample. The red, dashed line is the strong TDG candidate diagnostic line as defined in Sweet et al. (2014).

of them in this analysis. In essence this is because neither has a well-behaved mass-follows-light rotation curve: J1051-17:g11 has no detectable Hα on the southern semi-major axis, and a large correction for inclination; J1403-06:g1 has a disturbed rotation curve.

An improved strategy for identifying TDGs in this manner is: 1) measure metallicities with low-resolution spectra of as many galaxies as possible in a field, preferring those with easiest (edge-on) inclinations; and 2) measure rotational velocity with medium-resolution spectra of a subset of these, either optimising slit orientation for the high-metallicity candidates, or using an integral field spectrograph. In this way the effects of large inclination / position angle corrections can be minimised. However, this strategy does not take into account tidally disturbed or stripped matter at the outskirts of target galaxies, leading us to consider that problem in Section 4.

3.5 The apparently strongly-falling rotation curve of J0443-05:S4

As discussed in the previous sections, no galaxy in our sample that is a *strong* TDG candidate, based on elevated metallicity, exhibits a falling rotation curve. Relaxing the metallicity criterion somewhat, our next best candidate for a TDG based on metallicity and rotation curve is HIPASS J0443-05:S4 shown in Fig. 2. In terms of metallicity, this galaxy is 12+log(O/H)=8.86 and R-band magnitude M_R=-19.07, placing it within the metallicity-luminosity relation defined by the SDSS control sample. However, it is near

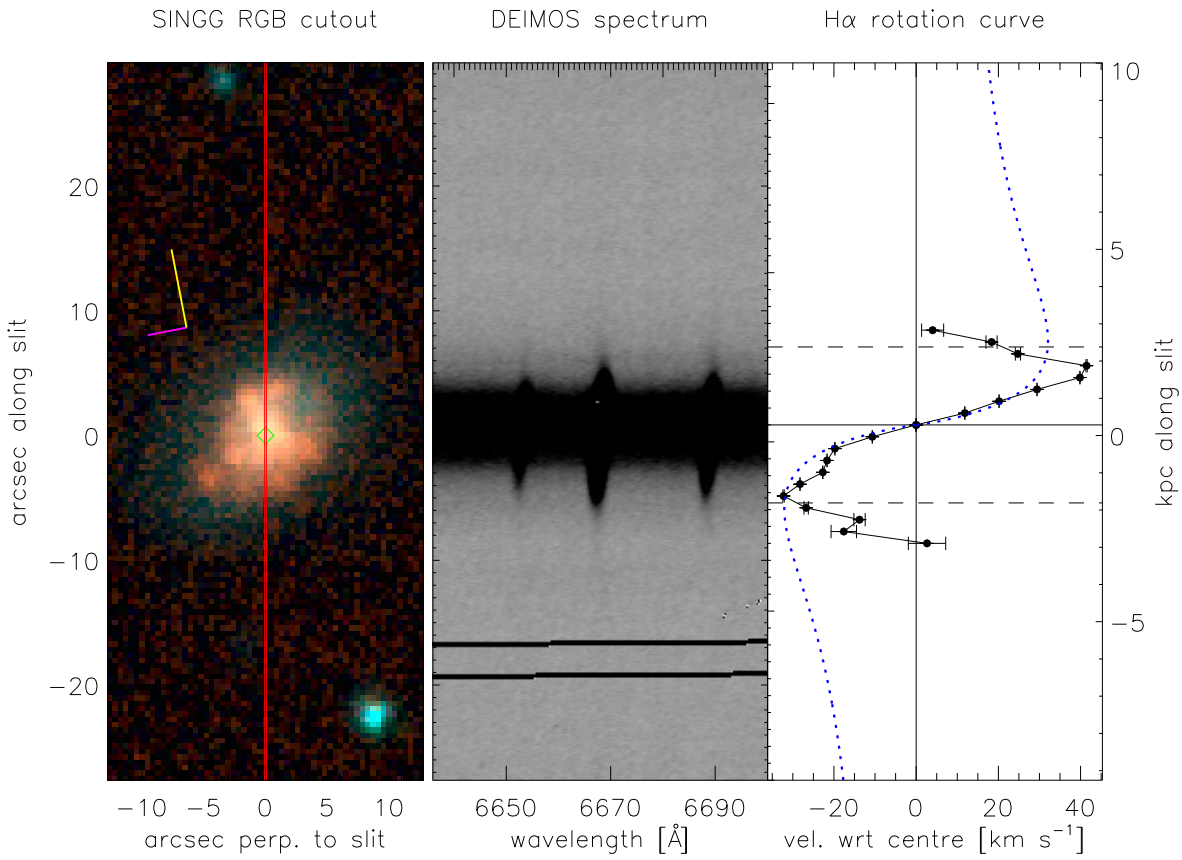

Figure 2. SINGG image, DEIMOS spectrum and rotation curve for HIPASS J0443-05:S4. (a) The left-most panel is the SINGG RGB image (R = R-band, G = narrow-band filter, B = net Hα). Stars appear cyan and HII regions appear red in this colour scheme. The red, vertical lines indicate the position of the slit, which runs the length of this panel. The compass shows N in yellow and E in magenta. The green diamond shows the optical (SINGG) centre of the object, corresponding to (0,0) on this plot. (b) The central panel is a cutout from the DEIMOS spectrum, showing Hα and [NII] emission lines. This covers the same angular height as the left-hand panel. (c) The right-hand panel is also the same angular height as the other two panels, with a matching kiloparsec scale on the right-hand axis. It contains the observed (uncorrected) rotation curve in black dots. The crosshairs are centered on the continuum flux peak centre, which is not necessarily the same as the optical centre in the left-hand panel. The dashed lines show the expected turnover radius $2r_0 = 1.2r_e$, assuming an exponential disk. The blue, dotted curve is a mass-follows-light rotational velocity prediction based on SINGG photometry and fitted to the observed rotation curve within the turnover radius. See text for details.

a giant spiral S2 which has a metallicity just 0.32 dex higher at 12+log(O/H)=9.18 and M_R=-22.57. We note that these differences in magnitude and metallicity are similar to those measured in the M31-M32 system (Δmag = 4.43; Δmetallicity = 0.22 dex; Richer et al. 1998), for which a tidal *encounter* has been proposed (e.g. Faber 1973; Bekki et al. 2001; Choi et al. 2002).

The measured rotation curve is falling rapidly beyond the turnover radius r_{turn}, indicating that dark matter is not *required* to explain its observed velocity (though it is not disallowed). In fact, the rotation curve shows a significant downturn *below* the mass-follows-light profile shown in blue, even reaching zero at the outskirts of the galaxy. This galaxy is near our nominal detection limit of $r_{tidal} = 2r_{turn}$, indicating that there could be some tidal warping of the rotation curve. However, the symmetry of this system indicates it is not subject to extreme tidal forces, so we do not believe that tides are causing the severe down-turn. The rapidly-falling rotation curve is not consistent with the predictions for a TDG, and the lack of evidence for tides corroborates this. The error bars (derived from the peak location error in the χ^2-minimisation fit to the Hα line) indicate that low S/N is not responsible for the unusual shape of this rotation curve. Nor can the downturn be attributed to instrumental signatures or residual sky lines; the same shape is observed for other emission lines in this system, which fall in other locations on the detector.

Clearly, a simplified disk model is not adequate to describe this galaxy. We propose two scenarios that may explain the stronger than Keplerian fall-off exhibited by the measured rotation curve: 1) polar ring galaxy, with a tilted inner structure and face-on outer disk; 2) kinematic twist due to a warped disk.

Firstly, we consider a polar ring galaxy, where the central, rising observed velocity profile belongs to a tilted inner bar, and the falling profile to a face-on outer disk with no measurable rotation. The observed morphology hints at a central bar, though more detailed imaging is required to confirm this. A polar ring structure like this is unusual in a dwarf (cf. De Rijcke et al. 2013), but could conceivably arise as a tilt to the galaxy's existing disk, triggered by an interaction with the neigbouring giant galaxy S2, if not the typical (for giant polar ring galaxies) method of accreting material from the nearby galaxy (Athanassoula & Bosma 1985). The size of the bar relative to the disk in this scenario is reminiscent of the morphological (cf. dynamical) bar of the LMC[3], as is the dwarf-giant separation ($\sim$ 50 kpc in both cases). van der Marel & Kallivayalil (2014) recently measured the LMC (stellar) rotation curve, but due to the high degree of scatter in the stellar velocities there is no clear trend in the outskirts of the galaxy with which to compare J0443-05:S4.

Our second hypothesis is that we are observing a kinematic twist or warp, where the kinematic position angle varies smoothly with radius (Krajnović et al. 2008). Kinematic and isophotal warps are caused by bars, often occurring with spiral arms (e.g. VCC0523, Ryś et al. 2013) or shells (e.g. Figure 5 of Emsellem et al. 2006). For a good visual example of an isophotal warp see Elmegreen et al. (1996), especially their Figure 1 (NGC1300 I). A warp of this magnitude would cause the line of nodes (region of zero velocity with respect to the systemic velocity) to lie at the edges of a poorly-aligned slit, mimicking a falling rotation curve such as we observe for J0443-05:S4. Indeed, the velocity profile along the minor axis of NGC1068 exhibits a falling rotation curve similar to ours (Emsellem et al. 2006).

To distinguish between these two degenerate scenarios we require additional data, in the form of integral field spectroscopy.

4 DISCUSSION: CAN THE FALLING ROTATION CURVES OF TDGS BE DETECTED?

In order to dynamically confirm a tidal dwarf galaxy by the absence of DM, when the M/L ratio is not known *a priori*, it is necessary to measure its velocity to sufficient radii to detect any fall in velocity, consistent with the predicted mass-follows-light model curve. In principle, because of the gradual, Keplerian fall-off, this translates to measurements of at least twice the turnover radius $r_{turn} = 1.2r_e$ for a pure exponential disk. This measurement becomes difficult at an exponential rate if it is assumed that our kinematics tracer of Hα emission has the same profile as continuum light (Dopita & Ryder 1994; Ryder & Dopita 1994). In practice, however, there are two bigger issues with measuring the rotation curve of a TDG.

[3] To be clear, the LMC is not considered by most to be a TDG.

Firstly, the Hα emission may be clumpy and more centrally-concentrated than the continuum light, making the measurement more difficult than predicted. We define the dynamical confirmation radius r_{det} as the maximum radius at which sensible fits to the emission in the spectra can be obtained (this translates to a S/N ratio of $\sim$ 3). This radius is a function mostly of the distribution of the Hα light but also influenced by the proximity to other SF regions (e.g. see the discussion for J1051-17:S7 in Appendix A). Identification becomes an issue if $2r_{turn} \gtrsim r_{det}$. This can be visualised in Figure 2 and Figures A1 to B12. If the Hα light is *less* centrally-concentrated than the continuum light, then this criterion works in our favour because the measurement at large radii is easier to make than for a simple exponential. Either way, one must assume that the velocity of HII regions is representative of the rotation curve. This will often be the case, even if the HII region is very large and non-central, as seen in Richards et al. (2014).

Secondly, the more critical issue is that the strong tidal fields that form a TDG, together with the low interior mass density expected for a DM-free TDG torn from the low-density outskirts of galaxies, lead to the tidal stripping of the outer baryonic matter of the TDG. With all other things equal, a normal galaxy with the same stellar mass as a TDG should be better able to survive tidal stretching because of its dark matter which increases its cohesion. Tidal stripping makes the measurement impossible when $2r_{turn} \gtrsim r_{tidal}$, where $r_{tidal} = 0.4d(m/M)^{1/3}$ is the tidal radius of the dwarf galaxy (for a fluid, triaxial satellite, as in Shu 1982); d = distance of closest approach, m = mass of dwarf galaxy, M = mass of giant host galaxy. It is worth noting that the velocity field will be disturbed even before the proximity criterion for stripping is reached, for instance Bekki & Couch (2011) showed that the rotation curve of a MW-type galaxy changes over time with tidal heating. As discussed in Renaud et al. (2009), tidal fields are in fact compressive as well as destructive; while the destructive stretching acts to pull galaxies apart, it is the compression mechanism that is responsible for the formation of TDGs. Aguilar & White (1986) also pointed out that while strong tidal encounters decrease the effective radius of a galaxy, weak encounters puff up the galaxy instead, e.g. by galaxy harassment (Moore et al. 1996). This disturbance is also problematic for a sound measurement of a rotation curve. However, we do not attempt to quantify this here for the sake of simplicity in this analysis.

We calculate r_{tidal} for each galaxy in our sample, assuming $d = \sqrt{2}d_{proj}$, where d_{proj} = projected distance to the nearest large galaxy, and the factor of $\sqrt{2}$ is based on a 45° projection angle. This assumes that the deprojected distance is the distance of closest approach. It is clearly very likely that this is not in fact the closest approach because the dwarf galaxies are more likely either on their way towards or away from the nearby giant, so will be closer in the future or have already been in the past. Therefore we are overestimating the tidal radius. For this calculation we also assume a M/L ratio for 'dwarfs' (galaxies with $M_R > -22$) of 1 $M_\odot/L_\odot$, and 4 $M_\odot/L_\odot$ for 'giant' ($M_R < -22$) galaxies, consistent with McGaugh & de Blok (1998); Toloba et al. (2011); Kalinova et al. (2013). This gives a mass ratio m/M of $1/4(l/L)$, where l and L are the

luminosity of the dwarf and giant galaxy respectively, so that $r_{tidal} = 0.4\sqrt{2}d_{proj}(l/4L)^{1/3}$.

In Fig. 4 we plot r_{tidal} vs. r_e; the dashed line indicates the required radius of $2r_{turn}$. Four of the 22 galaxies in our sample fall below this line, indicating that these could not be dynamically confirmed as tidal dwarf galaxies because no baryons should remain bound where the rotation curve is falling. A further five to six galaxies are borderline. Others in this sample could also be unidentifiable, given that the tidal radius is likely overestimated. Clearly, a large r_{tidal} is required for a galaxy to be dynamically confirmed to be a TDG; that is, the dwarf must be far from the nearest giant. However, the further away from the giant, the less likely the dwarf is to be formed in a tidal manner (c.f. J0443-05:S3, which has the largest r_{tidal} in the sample, and a flat (DM-rich) rotation curve, so is not a TDG). Further to this, we reiterate that the $2r_{turn}$ detection limit only indicates where the falling-velocity baryons do not remain bound. If a dwarf galaxy lies above this line then those baryons remain bound, but there must also be sufficiently bright Hα to meet the detectability radius r_{det} criterion before the galaxy can be detected as a TDG. Even with these DEIMOS observations only three (14%) galaxies have $r_{det} \gtrsim 2r_{turn}$ (shown as yellow pentagons in Fig. 4): J0443-05:S3, J1051-17:S5, J1059-09:S7. None of these has a falling rotation curve, so none is a TDG.

This effect is problematic for TDG candidates in the literature that have been identified based on their location within tidal streams, because the strong tides distort the rotation curves and dynamical M/L ratios. This is clear in the work by Mendes de Oliveira et al. (2001), who used velocity gradients to ascertain whether or not star-forming regions within tidal tails in Stephan's Quintet would remain bound, forming TDGs. None of the rotation curves shows a fall-off in velocity, and all are severely disturbed by the tidal field. The M/L ratios measured are inflated (5-73 $M_\odot/L_\odot$), requiring DM in opposition to expectations for TDGs. It may be argued that one can do better with HI measurements, probing to larger radii than Hα. Declining rotation curves are seen in some galaxies observed in HI including DDO 154 (Carignan & Purton (1998); Hoffman et al. (2001); however cf. de Blok et al. (2008)) and NGC 300 (Westmeier et al. 2011). In the case of DDO154, this measurement was possible because the galaxy is isolated and hence is not tidally truncated. However, this mass includes a substantial DM component and therefore rules out a tidal origin for this galaxy. Measurements of falling rotation curves remain difficult, except for a few select cases.

5 CONCLUSIONS

In this paper we presented DEIMOS observations of a sample of 22 star-forming dwarf galaxies in gas-rich groups. After prioritising our known group members in the slit mask design, we placed spare slits on as many sources as possible, with preference to galaxy-like photometry. In doing so we identified six additional small galaxies across two of the groups.

We measured the metallicity of those galaxies within our sample that have the necessary strong emission lines and found two new very strong TDG candidates (J1051-17:g11 and J1403-06:g1).

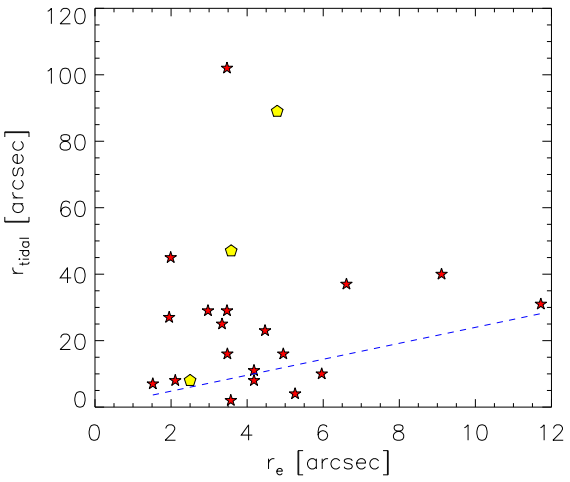

Figure 4. Tidal radius vs. effective radius for our sample of galaxies. See text for calculation of tidal radius. The dashed line indicates nominal detection limit of $2r_{turn} = 2.4r_e$. Below this limit it is not possible to dynamically confirm a falling rotation curve because baryons are tidally stripped down to $2r_{turn}$ (the radius at which a falling rotation curve may be detected). Yellow pentagons represent the galaxies in our sample that have measurable Hα beyond $2r_{turn}$; the galaxies that are not measurable at that radius are shown as red stars.

We constructed rotation curves for the dwarf galaxies in our sample and modelled them with a mass-follows-light fit to the central regions of each galaxy. All but one of the galaxies show signs of rotation with a mean of 39.3 km s^{-1} at r_{turn}, but most of the velocity profiles are disturbed so that a mass-follows-light profile does not fit the data, and neither does a mass-follows-light plus a DM component. The generally disturbed nature of the velocity profiles indicate that these galaxies are tidally perturbed.

M/L ratios in our sample are low ($0.73\pm0.39 M_\odot/L_\odot$), indicating that the stellar populations in these galaxies are young, consistent with their high rates of star-formation. There is some suggestion of a trend of M/L ratio with luminosity in our sample, with fainter galaxies having lower mass-to-light ratios.

One galaxy in our sample, J0443-05:S4, has an apparently strongly-falling rotation curve, reaching zero velocity at the outskirts of the galaxy. We propose that we may be observing either 1) a polar ring galaxy, with a tilted inner structure and face-on outer disk; 2) a kinematic twist due to a warped disk, with the line of nodes falling within the edges of the slit.

Even with very high sensitivity DEIMOS data, it remains difficult to convincingly measure the falling rotation curve of a TDG, due to both physical and observational effects. Observationally, the limitations of slit - galaxy position angle alignment severely constrain our ability to reliably measure kinematics of all galaxies in a group. To overcome these ob-

servational effects, integral field unit spectroscopy should be employed. For DEIMOS with a constraint of $\pm 30^\circ$, we have reliable measurements for 60% of our sample. This is considerably greater than the predicted 37.5%, suggesting that the position angles of the galaxies are aligned, perhaps due to group effects.

Physically, many of the rotation curves in our sample are disturbed due to recent interaction, or are not smooth due to having multiple star-forming regions. In addition to this, the outskirts of many of the dwarfs may be tidally stripped by interactions with neighbouring galaxies. As much as half of our sample could be affected by this. Even in the absence of tidal stripping, Hα light rapidly becomes progressively fainter beyond the turnover radius. Only 14% of our sample has detectable Hα light at sufficient radii to measure any fall in rotation curve; none of these has a falling rotation curve, so none is a TDG. It seems that falling rotation curves expected of TDGs can be detected only rarely, if at all.

ACKNOWLEDGEMENTS

We thank Peter Weilbacher and the anonymous referee for reviewing this paper.

We acknowledge funding support from the UQ-UWA Bilateral Research Collaboration Award and the Australian Research Council Discovery Project.

Some of the data presented herein were obtained at the W.M. Keck Observatory, which is operated as a scientific partnership among the California Institute of Technology, the University of California and the National Aeronautics and Space Administration. The Observatory was made possible by the generous financial support of the W.M. Keck Foundation. The authors wish to recognise and acknowledge the very significant cultural role and reverence that the summit of Mauna Kea has always had within the indigenous Hawaiian community. We are most fortunate to have the opportunity to conduct observations from this mountain.

This research has made use of the NASA's Astrophysics Data System.

This research has made use of the NASA/IPAC Extragalactic Database (NED) which is operated by the Jet Propulsion Laboratory, California Institute of Technology, under contract with the National Aeronautics and Space Administration.

This research has made use of the USNO Image and Catalogue Archive operated by the United States Naval Observatory, Flagstaff Station (http://www.nofs.navy.mil/data/fchpix/).

Table 1: Measured quantities for group member galaxies, including new group members. Columns (1) to (11).

(1) HIPASS+	(2) RA [h m s]	(3) Dec [d m s]	(4) reff ["]	(5) a/b	(6) PA [°]	(7) corr.	(8) M_R [mag]	(9) r_0 [kpc]	(10) I_0 [$L_\odot$/kpc]	(11) V_{hel} [km/s]
J0443-05:S3	04 44 11.67	-05 14 38.31	04.79±0.19	1.86	19	0.883	-19.93±0.19	1.809	2.3E+8	4591
J0443-05:S4	04 44 05.54	-05 25 46.50	04.95±0.12	1.6	120	0.537	-19.07±0.12	1.048	5.9E+8	4774
J1051-17:S3	10 51 35.94	-16 59 16.80	06.61±0.05	1.02	74	0.048	-18.14±0.05	2.232	4.7E+7	5969
J1051-17:S4	10 51 26.01	-17 05 03.61	03.48±0.09	1.4	164	0.661	-16.34±0.09	0.837	7.5E+7	5465
J1051-17:S5	10 51 50.91	-16 58 31.64	03.58±0.06	1.75	29	0.865	-17.20±0.06	0.842	1.9E+8	5465
J1051-17:S6	10 51 42.78	-17 06 34.59	02.11±0.04	1.29	40	0.422	-16.95±0.04	0.492	3.0E+8	5648
J1051-17:S7	10 51 33.36	-17 08 36.63	04.18±0.12	1.53	49	0.802	-16.94±0.12	0.799	1.2E+8	5374
J1051-17:S8	10 51 25.92	-17 08 16.44	04.47±0.10	3.07	63	0.927	-18.17±0.04	0.804	7.5E+8	5294
J1051-17:g04	10 51 39.679	-17 03 34.16	02.97±0.14	1.06	43	0.21	-18.10±0.05	1.45	5.0E+7	5535
J1051-17:g07	10 51 43.698	-17 01 42.99	03.34±0.09	1.12	42	0.3	-16.21±0.08	0.95	4.0E+7	6166
J1051-17:g11	10 51 40.051	-16 57 30.94	01.95±0.13	1	47	0.027	-16.37±0.11	0.28	1.3E+9	5371
J1051-17:g13	10 51 41.602	-17 05 20.16	01.52±0.16	1.05	42	0.21	-14.94±0.21	0.685	8.0E+6	5577
J1051-17:g15	10 51 33.286	-17 08 19.17	05.26±0.85	1.05	42	0.21	-15.18±0.81	2.63	4.0E+6	5225
J1059-09:S2	10 59 06.77	-09 45 04.38	11.72±0.24	1.36	131	0.056	-20.19±0.24	5.271	4.7E+7	8013
J1059-09:S5	10 59 30.98	-09 44 25.26	09.11±0.13	2.84	75	0.968	-19.94±0.13	2.973	2.4E+8	7926
J1059-09:S7	10 59 21.31	-09 47 50.49	02.50±0.15	1.59	115	0.167	-19.13±0.15	0.761	1.2E+9	7862
J1059-09:S8	10 59 01.73	-09 52 46.76	03.47±0.40	1.81	155	0.702	-16.98±0.40	1.028	9.4E+7	8260
J1059-09:S9	10 58 44.69	-09 53 28.60	01.99±0.08	1.39	45	0.604	-16.63±0.08	0.63	2.0E+8	8475
J1059-09:S10	10 59 02.64	-09 53 19.90	03.47±0.01	1.2	40	0.746	-20.95±0.01	4.11	5.0E+7	8219
J1403-06:S3	14 03 13.48	-06 06 24.17	04.18±0.85	1.03	14	0.158	-15.38±0.85	0.448	7.5E+7	2753
J1403-06:S4	14 03 34.62	-06 07 59.27	05.96±0.86	1.43	123	0.731	-14.51±0.86	0.961	1.4E+7	2671
J1403-06:g1	14 03 22.475	-06 00 44.24	03.57±0.36	2.04	46	0.76	-13.58±1.39	2.51	6.3E+6	2692

Columns: (1) SINGG name; (2) right ascension; (3) declination; (4) effective radius; (5) ratio of major to minor axes; (6) position angle; (7) velocity correction $\sin(i)\cos(\phi)$; (8) R-band extinction-corrected magnitude; (9) scale length; (10) central surface luminosity; (11) heliocentric velocity.

© 2014 RAS, MNRAS **000**, ??–??

Table 1: Measured quantities for group member galaxies, including new group members. Columns (12) to (22).

(1) HIPASS+	(12) Hβ	(13) [O III]	(14) Hα	(15) [N II]	(16) [S II]	(17) log(q)	(18) 12+log(O/H)	(19) A	(20) M/L [$M_\odot/L_\odot$]	(21) V_{rot} [km/s]	(22) r_{tidal} ["]
J0443-05:S3			10.5±2.1	0.8±0.4	3.4±1.5	7	$8.5\pm^{0.5}_{0.5}$	A	4.15	120	89
J0443-05:S4		28.2±8.8	174.8±1.0	46.9±0.4	69.6±1.5	6.89	$8.86\pm^{0.07}_{0.07}$	A	0.55	31.6	16
J1051-17:S3		7.2±0.7	19.0±0.2	2.8±0.2	8.6±1.0	6.8	$8.48\pm^{0.27}_{0.22}$			3.8	37
J1051-17:S4		5.0±0.6	9.8±0.1	0.4±0.1	3.8±1.3	6.91	$8.3\pm^{0.78}_{0.54}$	A	0.58	12.2	16
J1051-17:S5			32.4±0.4	2.9±0.3	12.4±0.7	7.13	$8.15\pm^{0.5}_{0.5}$	A	0.51	24.9	47
J1051-17:S6			162.2±2.1	22.5±0.6	49.3±2.0	7.15	$8.55\pm^{0.5}_{0.5}$	A	0.25	8.1	8
J1051-17:S7						0	$0\pm^{0}_{0}$	A	0.03	3.8	8
J1051-17:S8			4.7±0.1	3.9±0.2		0	$0\pm^{0}_{0}$	A	0.14	27.4	23
J1051-17:g04			19.3±0.4	6.7±0.4	15.0±0.6	7.58	$8.45\pm^{0.5}_{0.5}$			14.3	29
J1051-17:g07			15.0±0.4	2.4±0.4	5.1±1.6	7.82	$8.2\pm^{0.5}_{0.5}$			13.8	25
J1051-17:g11			0.7±0.1	0.5±0.2	1.5±0.2	7.85	$8.65\pm^{0.5}_{0.5}$			20.1	27
J1051-17:g13		13.0±2.3	11.9±0.2	0.7±0.2	3.4±0.6	6.99	$8.12\pm^{0.44}_{0.44}$			12	7
J1051-17:g15		134.6±48.8	12.4±0.2	1.7±0.2	7.8±1.4	6.82	$8.19\pm^{0.58}_{0.99}$			0	4
J1059-09:S2		41.9±6.9	43.3±0.7	6.3±0.4	17.6±1.1	6.99	$8.41\pm^{0.11}_{0.11}$			33.1	31
J1059-09:S5						0	$0\pm^{0}_{0}$	A	0.28	41.4	40
J1059-09:S7	10.4±0.2	13.0±2.0	65.9±1.0	14.8±0.3	23.8±0.9	6.9	$8.79\pm^{0.05}_{0.05}$			7.4	8
J1059-09:S8	1.3±0.3	3.2±1.5	6.5±0.3	1.2±0.1	2.6±0.4	7.02	$8.67\pm^{0.28}_{0.26}$	A	0.4	14.1	29
J1059-09:S9	1.4±0.1	7.5±1.4	9.0±0.3	0.7±0.1	4.0±0.4	6.91	$8.33\pm^{0.4}_{0.32}$	A	0.43	14.1	45
J1059-09:S10		4.7±0.7		9.3±1.3	2.0±1.1	9.49	$9.3\pm^{0.26}_{0.09}$			0.4	102
J1403-06:S3			9.9±0.1	0.6±0.1	2.4±0.1	7.29	$8.05\pm^{0.5}_{0.5}$			4.7	11
J1403-06:S4			2.4±0.1	0.2±0.1	0.6±0.1	7.38	$7.4\pm^{0.5}_{0.5}$			4.8	10
J1403-06:g1	3.3±0.1		21.5±0.2	5.7±0.2	6.9±0.1	7.56	$8.8\pm^{0.5}_{0.5}$			32.5	2

(12-16) observed flux for various emission lines in units of 10^{-22} erg s^{-1} cm^{-2}: [O III] λ5006.9, [N II] λ6583.4, [S II]$\lambda\lambda$6717.0+6731.3; (17) estimated ionization parameter basd on Dopita et al. (2013) interpolation if [OIII] available, or on M_R-log(q) relation of other galaxies in this sample otherwise; (18) 12+log(O/H) using Dopita et al. (2013) calibration; (19) Membership of Sample A (based on quality of rotation curve) is indicated here by the letter 'A'; (20) $R-$band mass-to-light ratio; (21) modelled rotational velocity at r_{turn}; (22) tidal radius.

© 2014 RAS, MNRAS **000**, ??–??

REFERENCES

Aaronson, M., Mould, J., & Huchra, J. 1980, ApJ, 237, 655
Aguilar, L. A., & White, S. D. M. 1986, ApJ, 307, 97
Athanassoula, E., & Bosma, A. 1985, ARAA, 23, 147
Barnes, D. G. et al. 2001, MNRAS, 322, 486
Bekki, K., & Couch, W. J. 2011, MNRAS, 415, 1783, 1105.0531
Bekki, K., Couch, W. J., Drinkwater, M. J., & Gregg, M. D. 2001, ApJL, 557, L39
Bell, E. F., McIntosh, D. H., Katz, N., & Weinberg, M. D. 2003, The Astrophysical Journal Supplement Series, 149, 289
Blumenthal, G. R., Faber, S. M., Primack, J. R., & Rees, M. J. 1984, Nature, 311, 517
Bournaud, F. 2010, Advances in Astronomy, 2010, 1
Bournaud, F. et al. 2007, Science, 316, 1166, 0705.1356
Braine, J., Duc, P.-A., Lisenfeld, U., Charmandaris, V., Vallejo, O., Leon, S., & Brinks, E. 2001, A&A, 378, 51, astro-ph/0108513
Carignan, C., & Purton, C. 1998, ApJ, 506, 125
Casas, R. A., Arias, V., Peña Ramírez, K., & Kroupa, P. 2012, MNRAS, 424, 1941
Choi, P. I., Guhathakurta, P., & Johnston, K. V. 2002, AJ, 124, 310
Clarke, C., & Oey, M. S. 2002, MNRAS, 337, 1299, astro-ph/0208442
de Blok, W. J. G., Walter, F., Brinks, E., Trachternach, C., Oh, S.-H., & Kennicutt, Jr., R. C. 2008, AJ, 136, 2648, 0810.2100
De Rijcke, S., Buyle, P., & Koleva, M. 2013, ApJL, 770, L26
Dopita, M., Hart, J., McGregor, P., Oates, P., Bloxham, G., & Jones, D. 2007, Astrophysics and Space Science, 310, 255, 0705.0287
Dopita, M. A., & Ryder, S. D. 1994, ApJ, 430, 163
Dopita, M. A., Sutherland, R. S., Nicholls, D. C., Kewley, L. J., & Vogt, F. P. A. 2013, ApJS, 208, 10
Drinkwater, M. J., Gregg, M. D., Hilker, M., Bekki, K., Couch, W. J., Ferguson, H. C., Jones, J. B., & Phillipps, S. 2003, Nature, 423, 519, arXiv:astro-ph/0306026
Duc, P. A., Brinks, E., Springel, V., Pichardo, B., Weilbacher, P., & Mirabel, I. F. 2000, The Astronomical Journal, 120, 1238
Duc, P.-A. et al. 2011, MNRAS, 417, 863
Duc, P.-A., Paudel, S., McDermid, R. M., Cuillandre, J.-C., Serra, P., Bournaud, F., Cappellari, M., & Emsellem, E. 2014, MNRAS, 440, 1458
Elmegreen, D. M., Elmegreen, B. G., Chromey, F. R., Hasselbacher, D. A., & Bissell, B. A. 1996, AJ, 111, 1880
Emsellem, E., Fathi, K., Wozniak, H., Ferruit, P., Mundell, C. G., & Schinnerer, E. 2006, MNRAS, 365, 367
Faber, S. M. 1973, ApJ, 179, 423
Faber, S. M. et al. 2003, in Society of Photo-Optical Instrumentation Engineers (SPIE) Conference Series, Vol. 4841, Instrument Design and Performance for Optical/Infrared Ground-based Telescopes, ed. M. Iye & A. F. M. Moorwood, 1657–1669
Freeman, K. C. 1970, Astrophysical Journal, 160, 811
Gibson, B. K., & Matteucci, F. 1997, Astrophysical Journal v.475, 475, 47
Gómez, P. L. et al. 2003, ApJ, 584, 210
Hoffman, G. L., Salpeter, E. E., & Carle, N. J. 2001, AJ, 122, 2428, astro-ph/0107484
Kalinova, V., van de Ven, G., Lyubenova, M., Falcon-Barroso, J., & van den Bosch, R. 2013, in American Astronomical Society Meeting Abstracts, Vol. 221, American Astronomical Society Meeting Abstracts 221, 241.05
Kauffmann, G. et al. 2003, MNRAS, 346, 1055
Klypin, A., Zhao, H., & Somerville, R. S. 2002, ApJ, 573, 597, astro-ph/0110390
Krajnović, D. et al. 2008, MNRAS, 390, 93
Lequeux, J., Peimbert, M., Rayo, J. F., Serrano, A., & Torres-Peimbert, S. 1979, Astronomy & Astrophysics, 80, 155
Lewis, I. et al. 2002, MNRAS, 334, 673
Marino, R. A. et al. 2013, A&A, 559, A114
McGaugh, S. S., & de Blok, W. J. G. 1998, ApJ, 499, 41
Mendes de Oliveira, C., Plana, H., Amram, P., Balkowski, C., & Bolte, M. 2001, AJ, 121, 2524
Meurer, G. R. et al. 2006, ApJS, 165, 307
Mirabel, I. F., Dottori, H., & Lutz, D. 1992, Astronomy and Astrophysics (ISSN 0004-6361), 256, L19
Moore, B., Katz, N., Lake, G., Dressler, A., & Oemler, A. 1996, Nature, 379, 613, astro-ph/9510034
Navarro, J. F. 1998, ArXiv Astrophysics e-prints, astro-ph/9807084
Oey, M. S. et al. 2007, ApJ, 661, 801, astro-ph/0703033
Oppenheimer, B. D., Davé, R., Kereš, D., Fardal, M., Katz, N., Kollmeier, J. A., & Weinberg, D. H. 2010, MNRAS, 406, 2325, 0912.0519
Peebles, P. J. E. 1965, ApJ, 142, 1317
Penny, S. J., Conselice, C. J., de Rijcke, S., & Held, E. V. 2009, MNRAS, 393, 1054
Press, W. H., & Schechter, P. 1974, ApJ, 187, 425
Renaud, F., Boily, C. M., Naab, T., & Theis, C. 2009, ApJ, 706, 67
Richards, S. N. et al. 2014, MNRAS, 445, 1104, 1409.4495
Richer, M., McCall, M. L., & Stasińska, G. 1998, A&A, 340, 67
Rodríguez-González, A., Esquivel, A., Velázquez, P. F., Raga, A. C., & Melo, V. 2008, ApJ, 689, 153, 0808.1611
Ryder, S. D., & Dopita, M. A. 1994, ApJ, 430, 142
Ryś, A., Falcón-Barroso, J., & van de Ven, G. 2013, MNRAS, 428, 2980
Searle, L., & Zinn, R. 1978, ApJ, 225, 357
Shopbell, P. L., & Bland-Hawthorn, J. 1998, ApJ, 493, 129, astro-ph/9708038
Shu, F. H. 1982, The Physical Universe (University Science Books)
Sweet, S. M., Drinkwater, M. J., Meurer, G., Bekki, K., Dopita, M. A., Kilborn, V., & Nicholls, D. C. 2014, The Astrophysical Journal, 782, 35
Sweet, S. M. et al. 2013, Monthly Notices of the Royal Astronomical Society, 433, 543
Toloba, E., Boselli, A., Cenarro, A. J., Peletier, R. F., Gorgas, J., Gil de Paz, A., & Muñoz-Mateos, J. C. 2011, A&A, 526, A114
Tremonti, C. A. et al. 2004, ApJ, 613, 898
Tully, R. B., & Fisher, J. R. 1977, A&A, 54, 661
van den Bergh, S. 1988, PASP, 100, 344
van der Marel, R. P., & Kallivayalil, N. 2014, ApJ, 781, 121
Weilbacher, P. M., Duc, P.-A., & Fritze-v. Alvensleben, U. 2003, A&A, 397, 545

Westmeier, T., Braun, R., & Koribalski, B. S. 2011, MNRAS, 410, 2217, 1009.0317

APPENDIX A: SAMPLE A

A1 Notes on individual galaxies

J0443-05:S3 (Figure A1). This galaxy is the most 'normal' in our sample, with a small stellar bulge (cyan) surrounded by a star-forming disk (red), and a flat rotation curve, consistent with a DM halo. Its tidal radius is much larger than its effective radius, borne out by the large radius to which we measure a typical rotation curve. It also has the highest M/L ratio in our sample at $4.15 M_{\odot}/L_{\odot}$.

J0443-05:S4 (Figure 2). This galaxy has a stronger than Keplerian fall-off in its rotation curve. It is depicted in Figure 2 and is discussed in detail in Section 3.5.

J1051-17:S4 (Figure A2). This galaxy has three separate SF regions, with velocity rising linearly with position along slit, consistent with solid body rotation. The observed rotation rises above the model predictions, suggestive of the presence of DM. It has a low M/L ratio ($0.58 M_{\odot}/L_{\odot}$), consistent with most of the dwarfs in our sample.

J1051-17:S5 (Figure A3). There appear to be two SF regions in this galaxy. The velocity profile of this galaxy is not well fit by the canonical mass-follows-light rotation curve. However, this galaxy is not likely suffering from tidal effects due to its position on the $r_{tidal} - r_e$ plot.

J1051-17:S6 (Figure A4). This galaxy has a velocity similar to the disk of the nearby giant S1. The observed velocity profile of S6 is distorted beyond r_{turn} by its proximity to S1.

J1051-17:S7 (Figure A5). S7 is the brighter feature to the W of the slit (that is, the bottom of this figure). Also measured in this slit is an HII region in the plane of the disk of S1 ('S7a'), towards the top of this figure. The velocity profile shown here is that of S7 only. It is disrupted, consistent with this galaxy having recently passed through the disk of S1 and possibly inducing star formation in S7a. Its velocity is clearly offset from the velocity of the neighbouring disk of S1, but the shape of the spiral arm of S1 passing near S7 is distorted and the Hα emission is enhanced, strongly suggesting a recent interaction.

J1051-17:S8 (Figure A6). The velocity profile of this galaxy is consistent with a mass-follows-light profile with a kinematically decoupled core. The faint Hα emission and bright continuum at the centre makes the velocity profile difficult to measure beyond the region shown here, especially at the NE end of the slit. The apparent Hα absorption in the central panel is in fact an adjacent, poorly-subtracted sky line.

J1059-09:S5 (Figure A7). For this slit, Hα and [NII] lines fall on the edge of the CCD, so we opt for the [OIII] λ5007 line in our kinematical analysis in order to avoid possible edge of frame effects. Similar observations with a slit better placed with respect to the mask centre would result in Hα kinematics extending $\sim$1 kpc beyond what we show for [OIII] 5007. The observed velocity rises above the model curves, suggestive of the presence of DM.

J1059-09:S8 (Figure A8). Mass follows light for this small galaxy. It has a metallicity 2.5σ above the SDSS mean for its luminosity, so is close to our TDG selection limit. Moreover, it is near in projection to the very high metallicity dwarf S10 and may be related to it.

J1059-09:S9 (Figure A9). This small galaxy has very low surface brightness.

A2 Figures

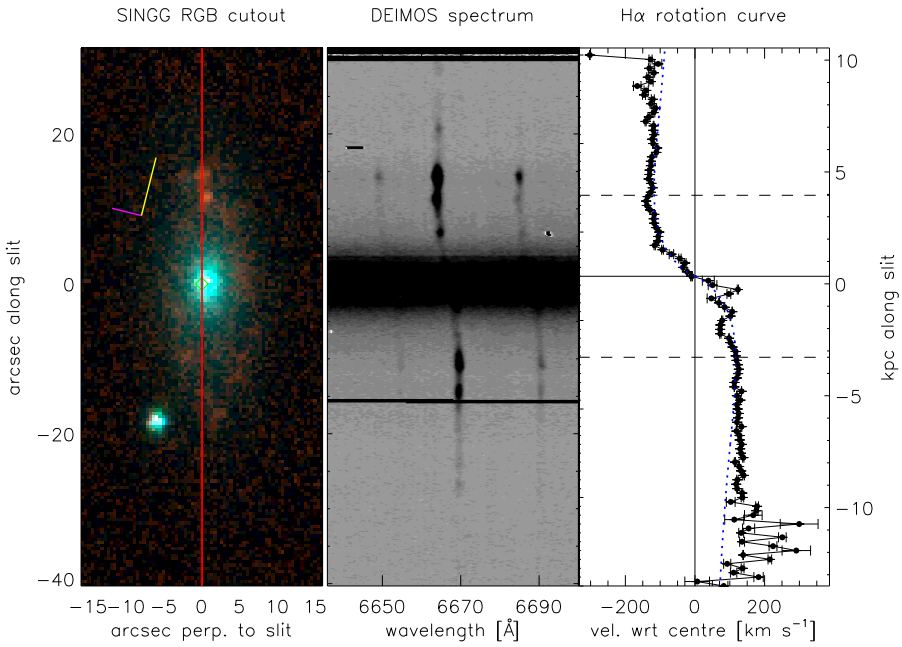

Figure A1. J0443-05:S3. As for Figure 2.

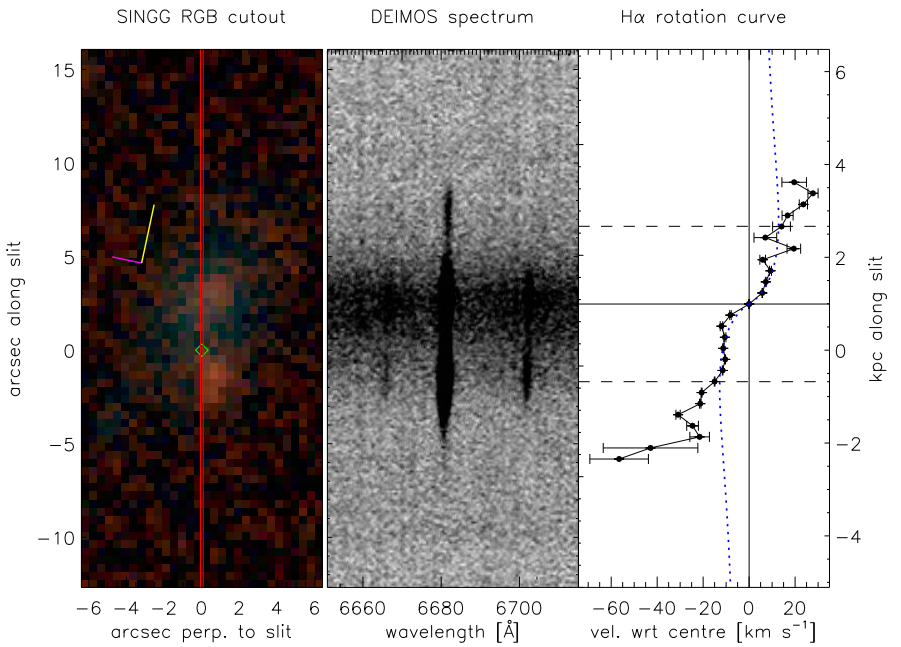

Figure A2. J1051-17:S4. As for Figure 2.

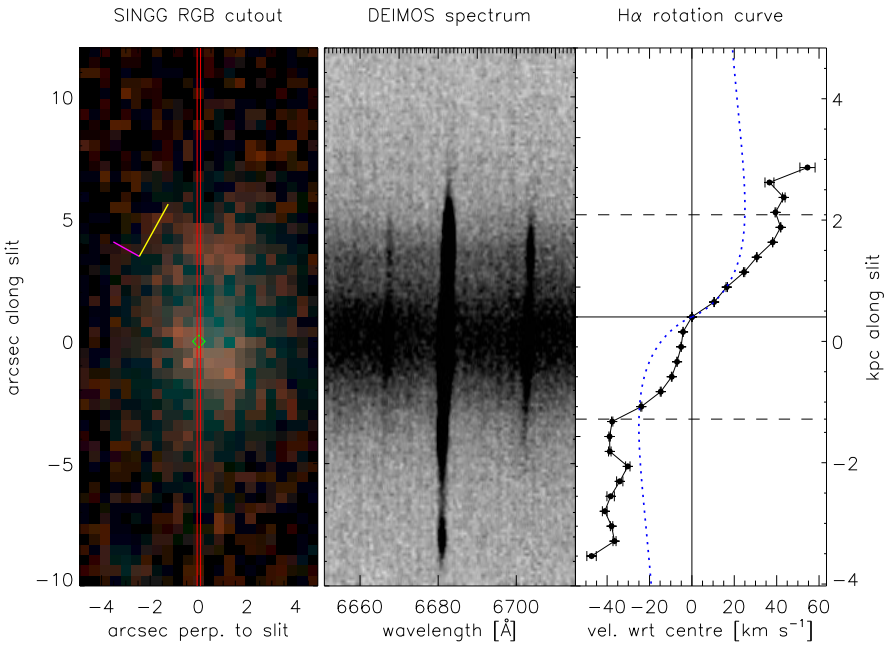

Figure A3. J1051-17:S5. As for Figure 2.

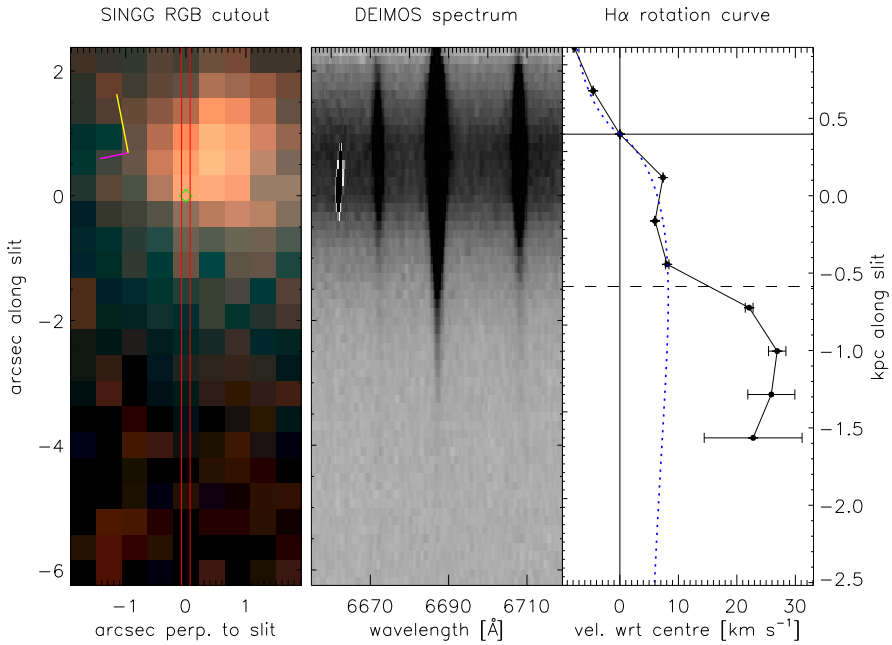

Figure A4. J1051-17:S6. As for Figure 2.

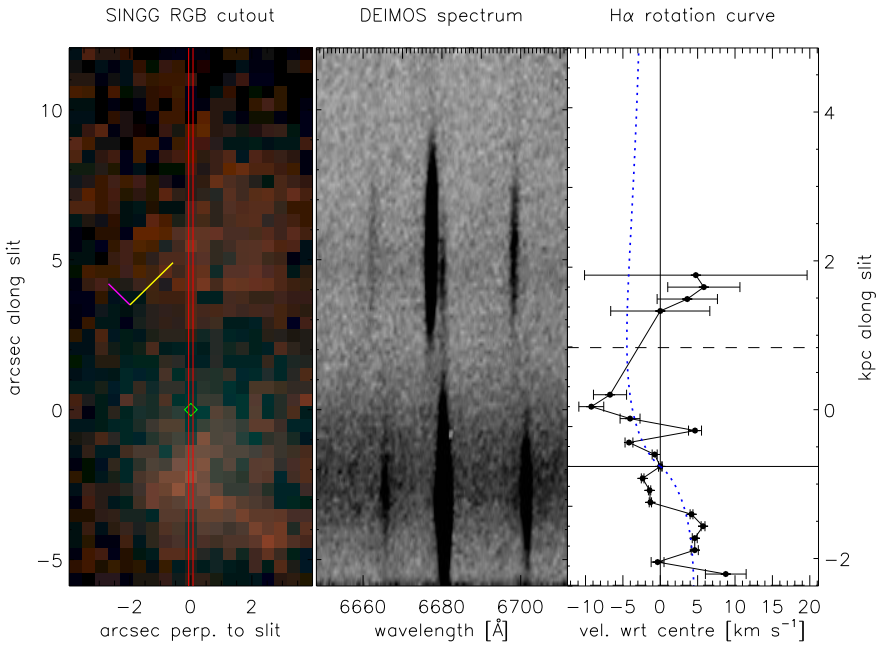

Figure A5. J1051-17:S7. As for Figure 2.

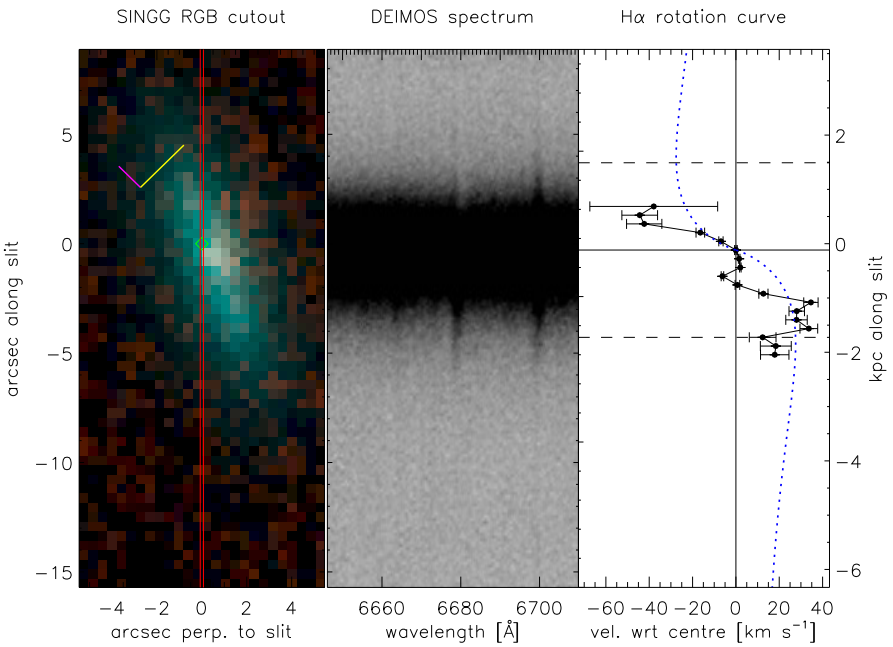

Figure A6. J1051-17:S8. As for Figure 2.

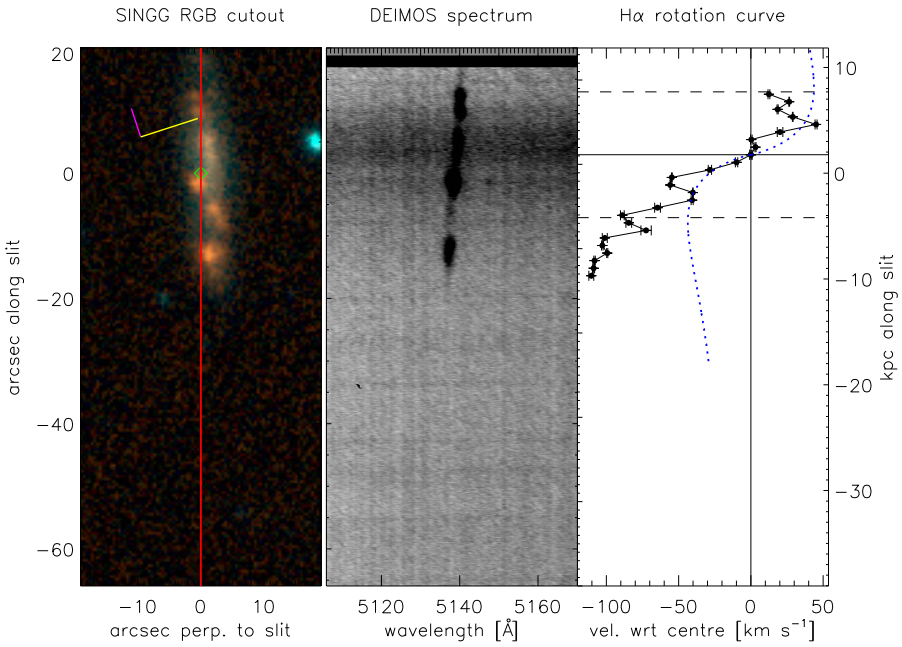

Figure A7. J1059-09:S5. As for Figure 2.

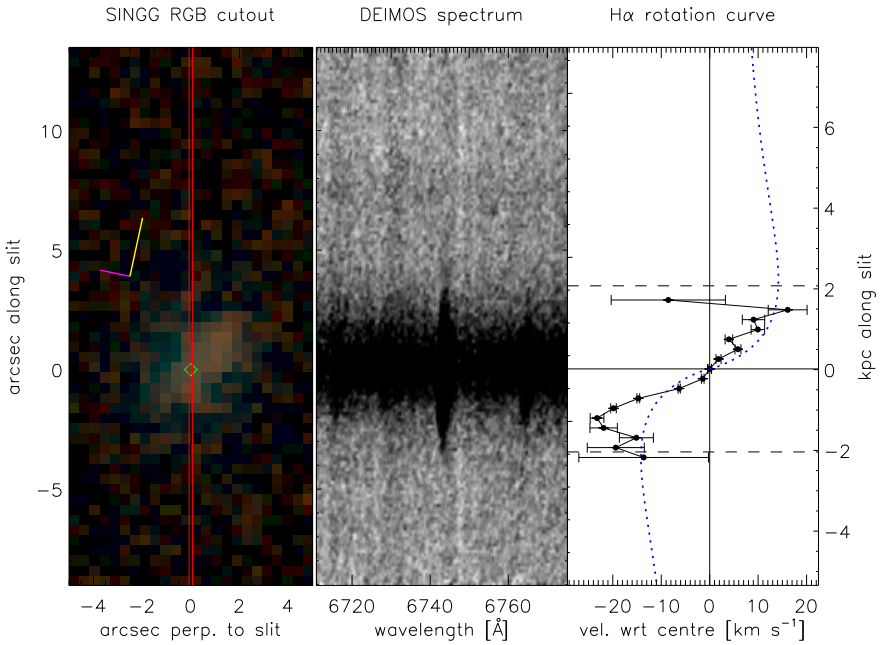

Figure A8. J1059-09:S8. As for Figure 2.

© 2014 RAS, MNRAS **000**, ??–??

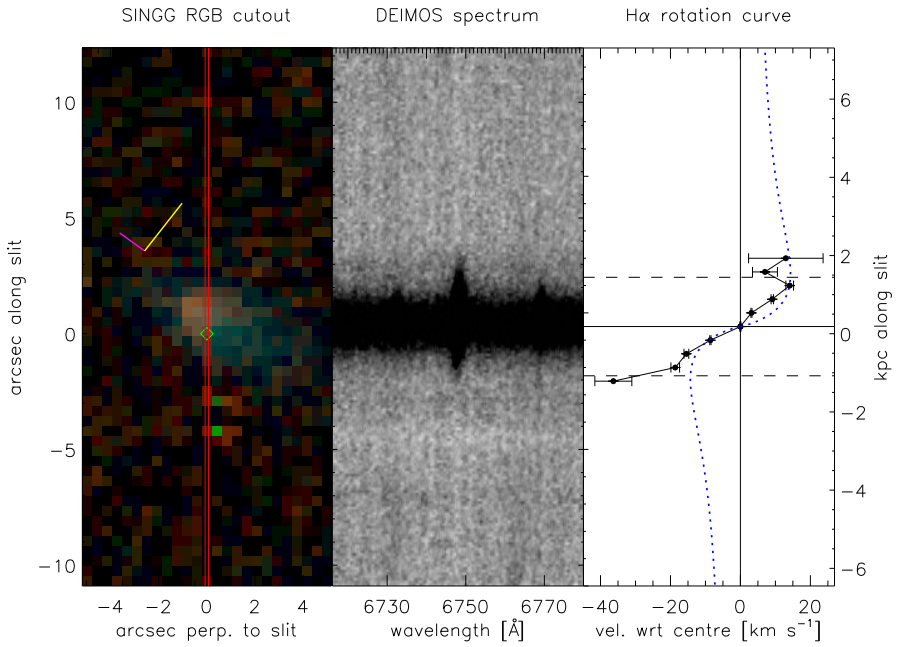

Figure A9. J1059-09:S9. As for Figure 2.

APPENDIX B: SAMPLE B

B1 Notes on individual galaxies

J1051-17:S3 (Figure B1). This galaxy is face-on, so no meaningful velocity profile is measurable.

J1051-17:g04 (Figure B2). The misalignment between optical and slit PAs prohibits sound measurement of this small, newly-identified galaxy.

J1051-17:g07 (Figure B3). This new, faint galaxy has strong Hα emission but very faint continuum.

J1051-17:g11 (Figure B4). For this new galaxy there is a very large correction for inclination and orientation. There are no observed data points below the continuum centre in Figure B4 because there is insufficient Hα light on this side of the galaxy. Its high metallicity leads us to classify this galaxy as a very strong TDG candidate.

J1051-17:g13 (Figure B5). This galaxy's inclination is uncertain, so it is difficult to measure its mass-to-light ratio. Its velocity profile appears to be disturbed.

J1051-17:g15 (Figure B6). This galaxy has very low surface brightness, so is barely evident in the SINGG image. Its extent in Hα is well below the tidal truncation size and the velocity structure along the slit is erratic but has low amplitude.

J1059-09:S2 (Figure B7). This clumpy galaxy is consistent with a mass-follows-light profile. Note that the large corrections for slit position angle and galaxy inclination contribute to the large M/L ratio.

J1059-09:S7 (Figure B8). The velocity profile of this galaxy has a very unusual shape. It is very near the interacting galaxies S1 and S3, so is likely disturbed by their tides. Moreover, the slit is close to aligning with the minor axis of this galaxy, so the kinematics may be indicative of a galactic wind.

J1059-09:S10 (Figure B9). This galaxy has a very strong stellar component (as evidenced by the blue colour in Figure B9). Its rotation curve is not well fit by a predicted mass-follows-light relation. The galaxy has a possible counter-rotating Hα absorption component, the analysis of which is beyond the scope of the paper. It has a fairly high metallicity consistent with a TDG, though not above our diagnostic cut. However, it is not near a host, so must be an old TDG if it is one. It is near another dwarf (S8) of metallicity $\sim$2.5-σ above the SDSS control sample.

J1403-06:S3 (Figure B10). This slit measures an offset HII region within a very low surface brightness dwarf galaxy, so it is difficult to claim that this galaxy is rotating. It is only marginally detectable based on our r_{tidal} detection limit, and indeed we do not measure rotation past r_{turn}.

J1403-06:S4 (Figure B11). This very low surface brightness galaxy consists of two SF regions likely disturbed by the two giant interacting galaxies S1 and S2. It is sufficiently small to lie below the detection limit set by r_{tidal}.

J1403-06:g1 (Figure B12). This appears to be a giant HII region within the halo of the giant galaxy S2. It has high metallicity consistent with a TDG, but a very warped rotation curve. Due to its small size and proximity to S2, it is well below the tidal stripping detection limit.

B2 Figures

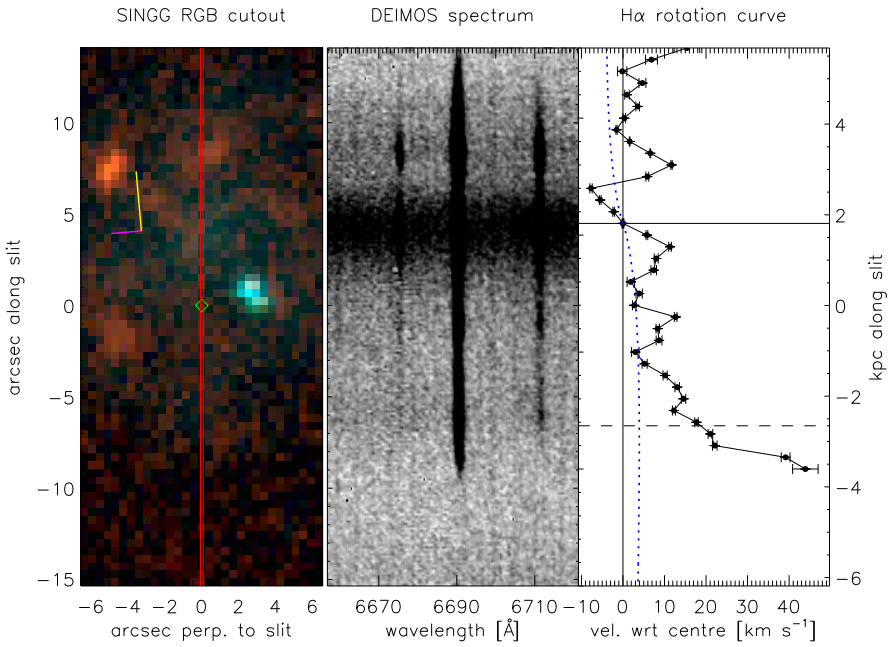

Figure B1. J1051-17:S3. As for Figure 2.

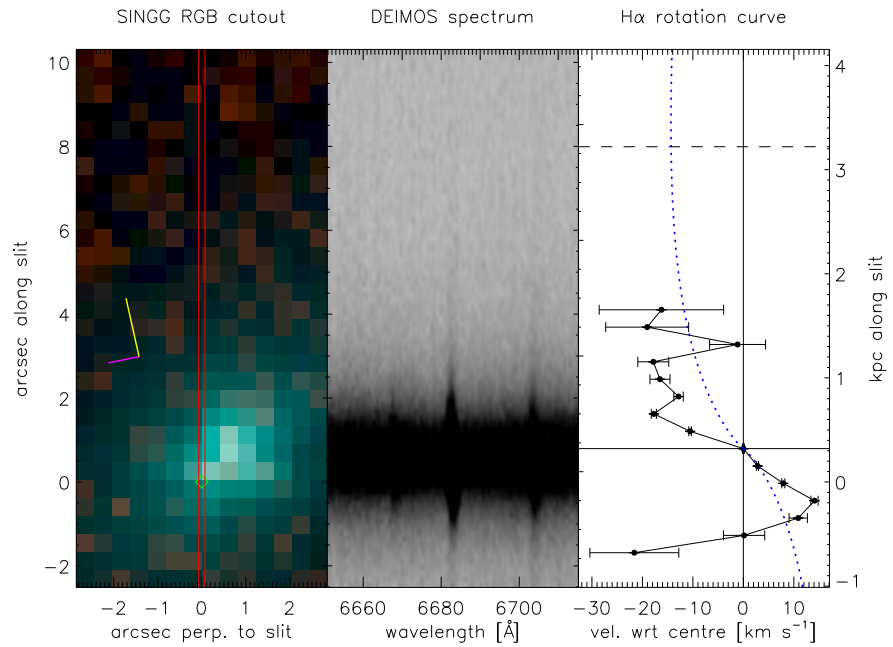

Figure B2. J1051-17:g04. As for Figure 2.

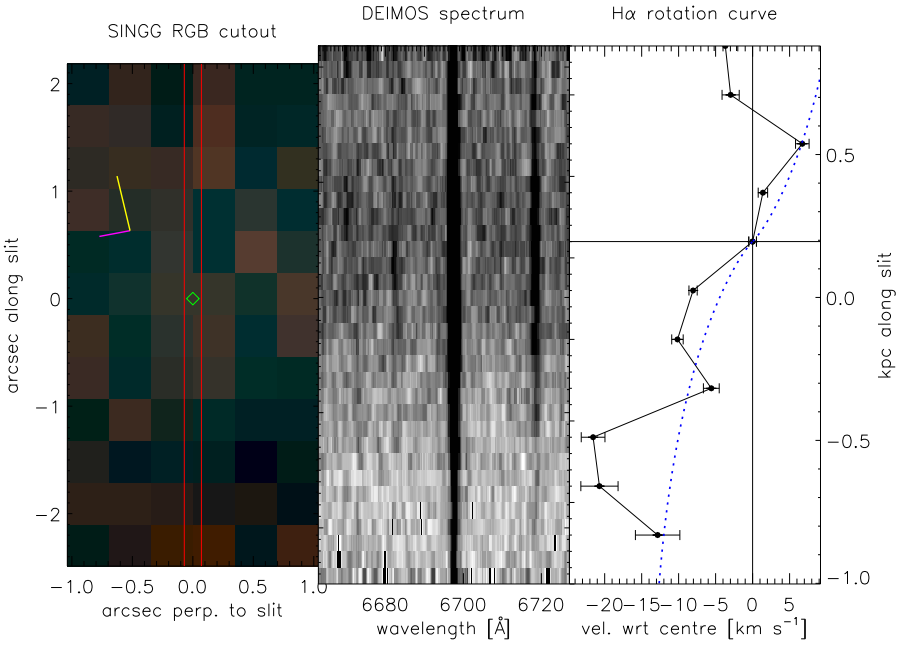

Figure B3. J1051-17:g07. As for Figure 2.

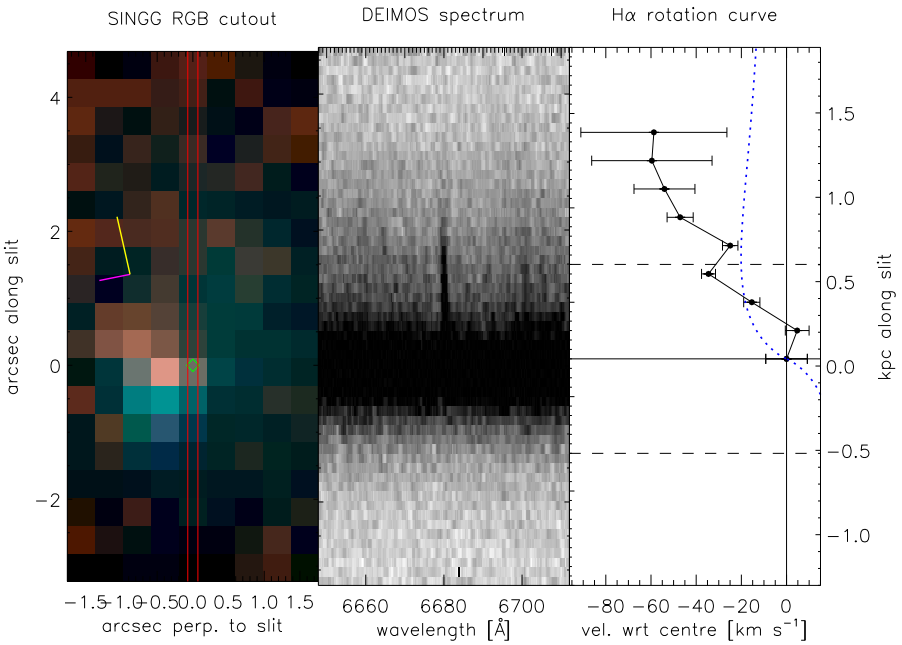

Figure B4. J1051-17:g11. As for Figure 2.

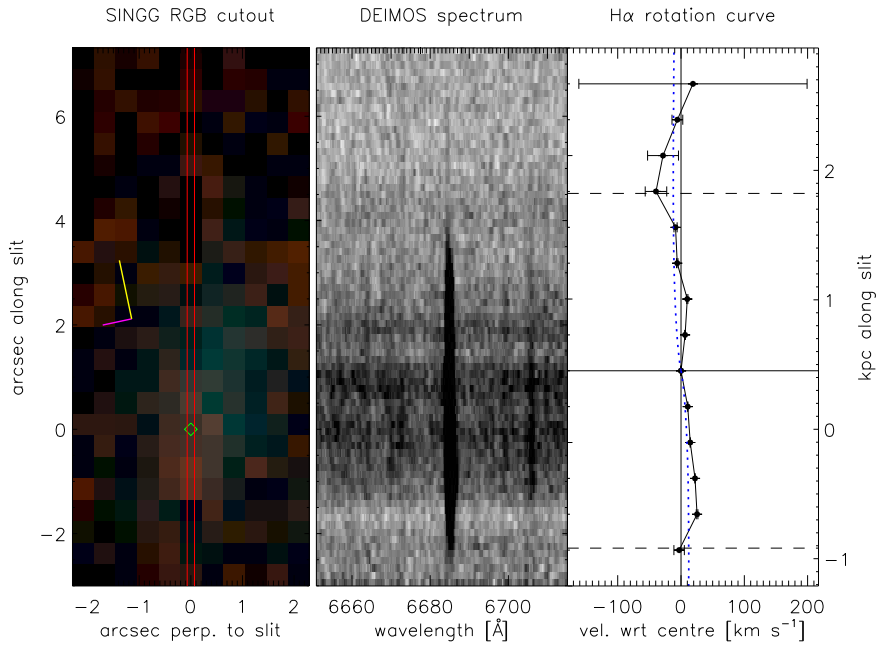

Figure B5. J1051-17:g13. As for Figure 2.

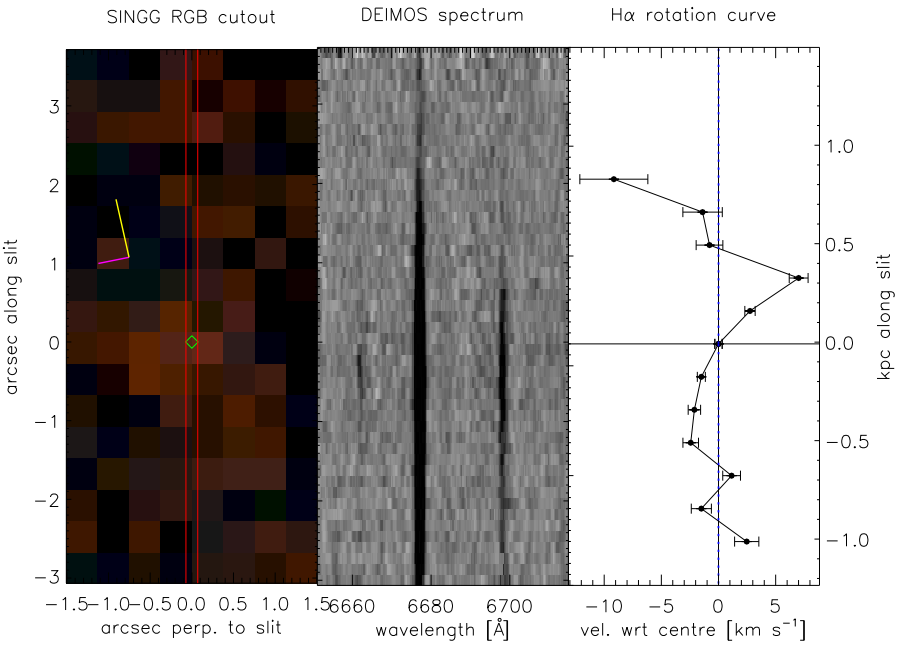

Figure B6. J1051-17:g15. As for Figure 2.

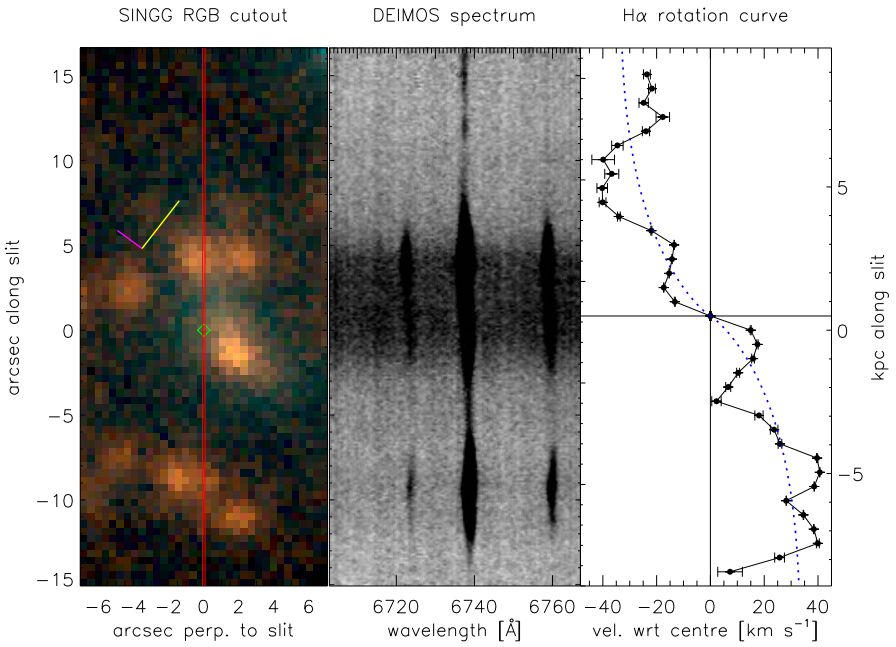

Figure B7. J1059-09:S2. As for Figure 2.

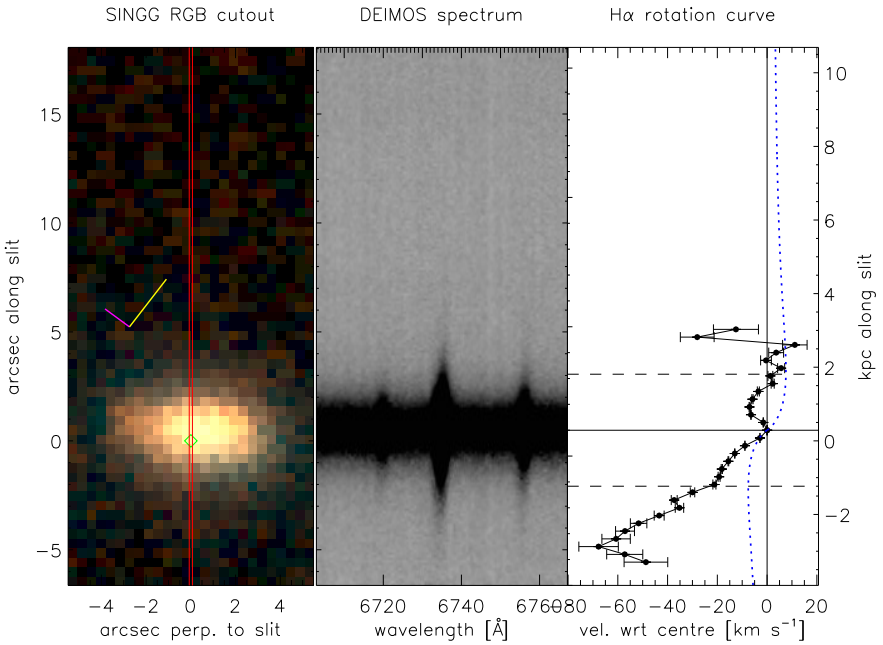

Figure B8. J1059-09:S7. As for Figure 2.

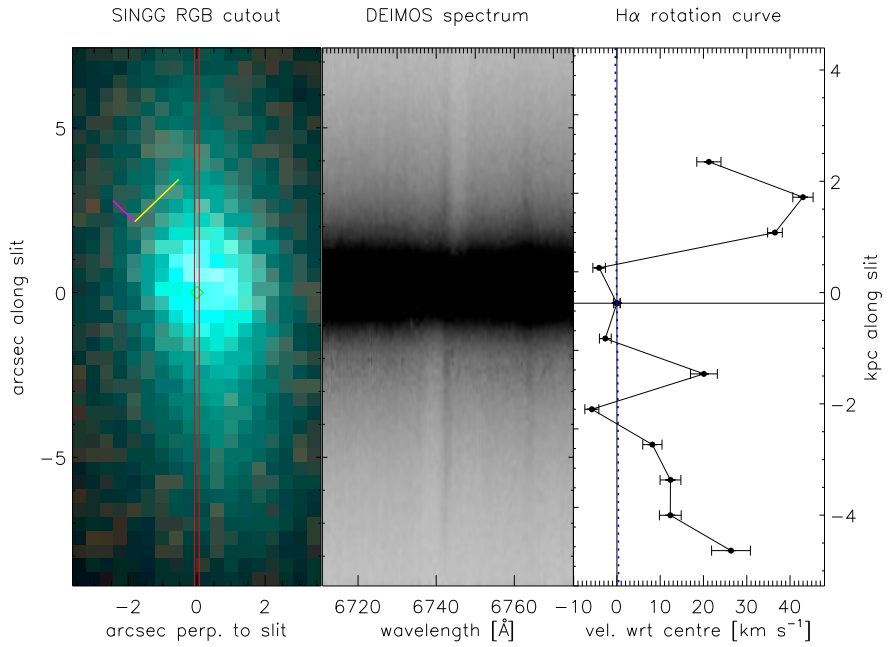

Figure B9. J1059-09:S10. As for Figure 2.

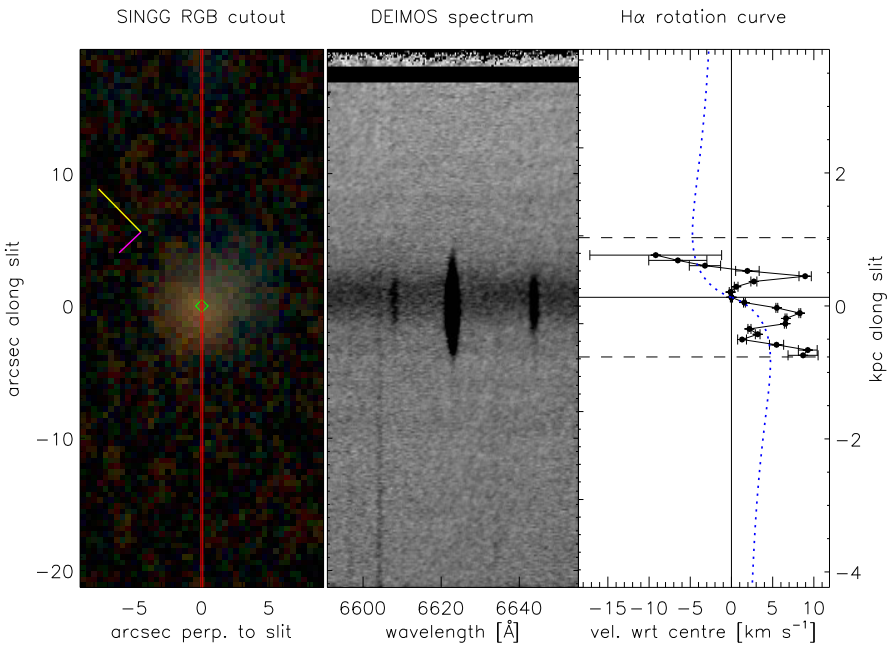

Figure B10. J1403-06:S3. As for Figure 2.

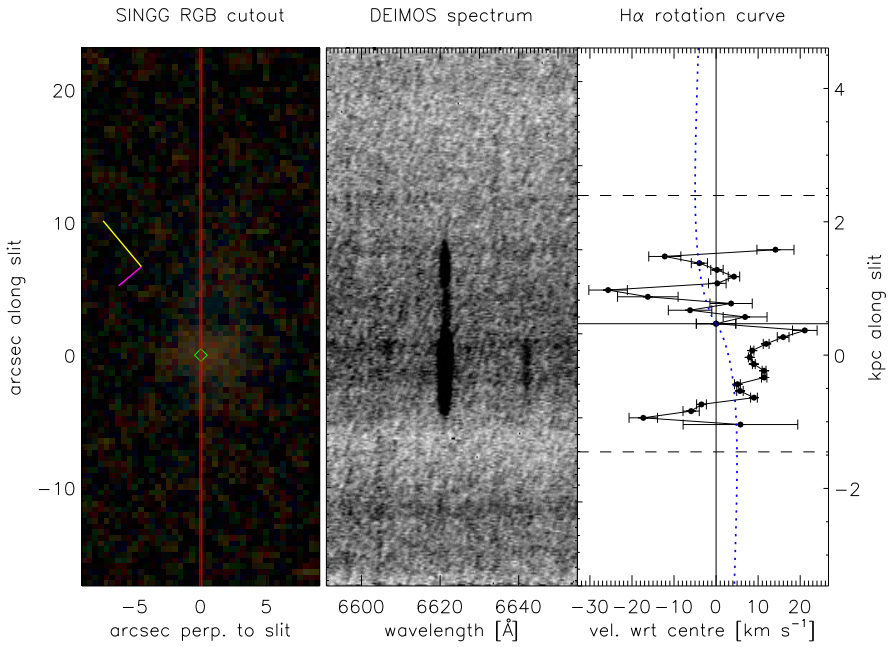

Figure B11. J1403-06:S4. As for Figure 2.

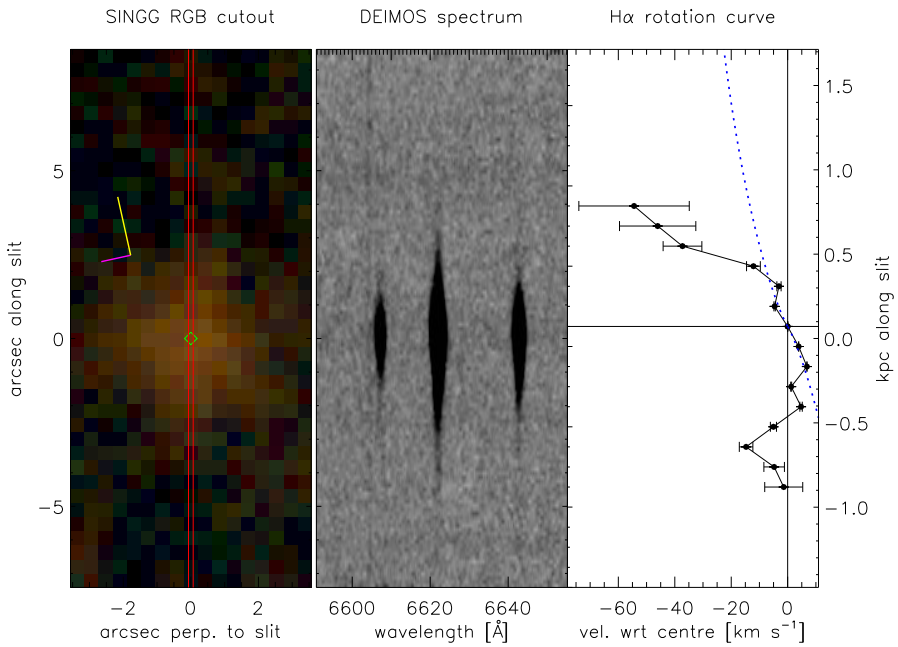

Figure B12. J1403-06:g1. As for Figure 2.

APPENDIX C: MASK AND SLIT PLACEMENT

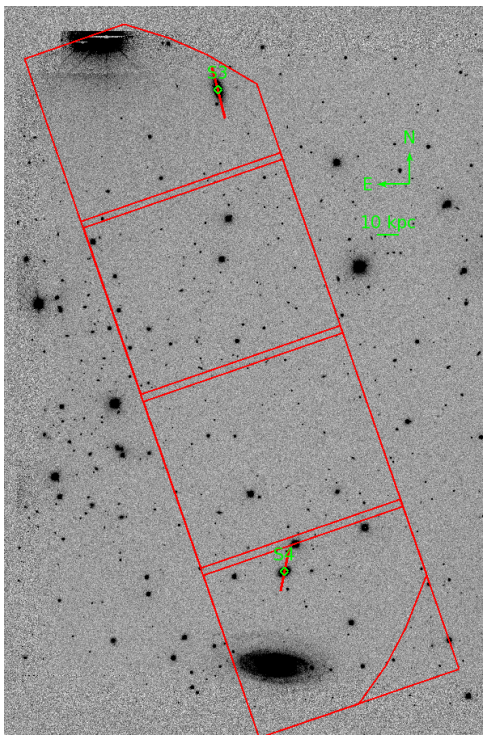

Figure C1. SINGG image of HIPASS J0443-05 showing locations of slits (red) for measured galaxies (green labels). The approximate location of the DEIMOS mask is given by the red polygon. The other slits are not shown for clarity.

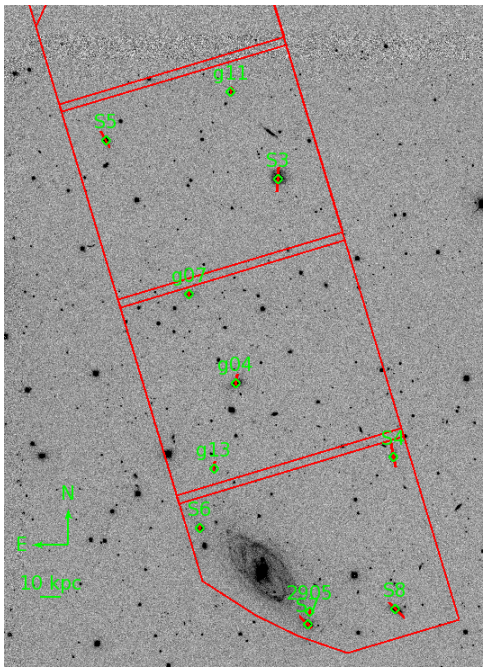

Figure C2. SINGG image of HIPASS J1051-17 showing locations of slits (red) for measured galaxies (green labels). The approximate location of the DEIMOS mask is given by the red polygon. The other slits are not shown for clarity.

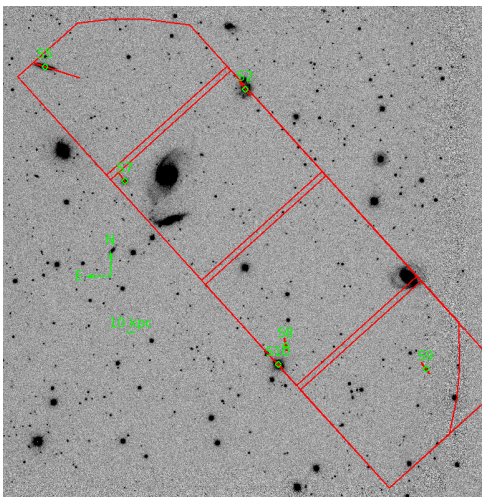

Figure C3. SINGG image of HIPASS J1059-09 showing locations of slits (red) for measured galaxies (green labels). The approximate location of the DEIMOS mask is given by the red polygon. The other slits are not shown for clarity.

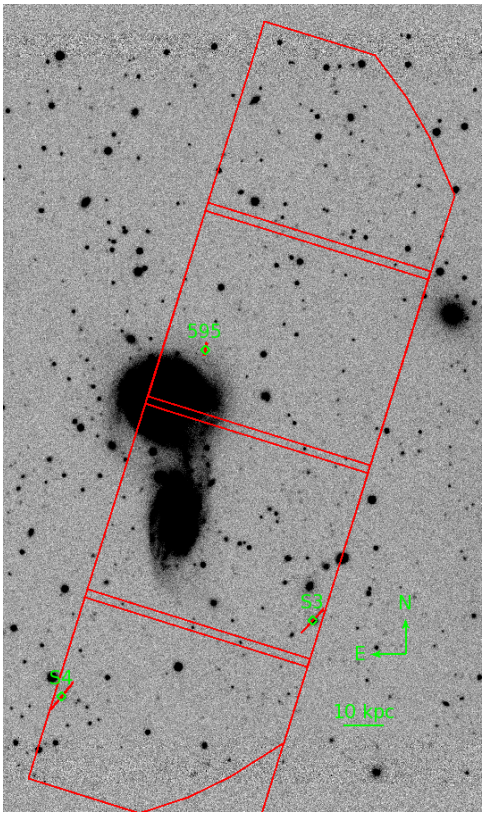

Figure C4. SINGG image of HIPASS J1403-06 showing locations of slits (red) for measured galaxies (green labels). The approximate location of the DEIMOS mask is given by the red polygon. The other slits are not shown for clarity.